https://doi.org/10.5194/egusphere-2024-3029
Preprint. Discussion started: 8 October 2024

Trends and seasonal signals in Atlantic feature-based jet stream characteristics and in weather types.

Hugo Banderier[1,2], Alexandre Tuel[3], Tim Woollings[4], and Olivia Martius[1,2,5]

[1]Institute of Geography, University of Bern, Bern, Switzerland
[2]Oeschger Centre for Climate Change Research, University of Bern, Bern, Switzerland
[3]Galeio, Paris, France
[4]Atmospheric, Oceanic and Planetary Physics, University of Oxford, Oxford, United Kingdom
[5]Mobiliar Lab for Natural Risks, University of Bern, Bern, Switzerland

Correspondence: Hugo Banderier (hugo.banderier@unibe.ch)

Abstract. Recent studies have highlighted the link between upper-level jet dynamics, especially the persistence of certain jet configurations, and extreme summer weather in Europe. The weaker and more variable nature of the jets in summer makes it difficult to apply the tools developed to study them in winter, at least not without modifications. Here, to further investigate the link between jets and persistent summer weather, we present two complementary approaches to characterize the jet dynamics in the North Atlantic sector and use them primarily on the summer circulation.

First, we apply the self-organizing map (SOM) clustering algorithm to create a 2D distance-preserving discrete feature space to the tropopause-level wind field over the North Atlantic. The dynamics of the tropopause-level wind can then be described by the time series of visited SOM clusters, in which a long stay in a given cluster relates to a persistent state and a rapid transition between clusters that are far apart relates to a sudden considerable shift in the configuration of upper-level flow.

Second, we adapt and apply a jet axis detection and tracking algorithm to extract individual jets and classify them in the canonical categories of eddy-driven and subtropical jets (EDJ and STJ, respectively). Then, we compute a wide range of jet indices on each jet to provide easily interpretable scalar time series representing upper-tropospheric dynamics.

This work will exclusively focus on the characterization of historical trends, seasonal cycles, and other statistical properties of the jet stream dynamics, while ongoing and future work will use the tools presented here and apply them to the study of connections between jet dynamics and extreme weather. The SOM allows the identification of specific jet configurations, each one representative of a large number of days in historical time series, whose frequency or persistence had increased or decreased in the last decades. Detecting and categorizing jets adds a layer of interpretability and precision to previously and newly defined jet properties, allowing for a finer characterization of their trends and seasonal signals.

Detecting jets on flattened pressure levels instead the 2PVU surface is more robust in summer, and finding wind-direction-aligned subsets of 0-contours in a wind shear field is a fast and robust way to extract jet features. Using the SOM, we highlight a trend towards more negative NAO, and isolate predictable and/or persistent circulation patterns. Using properties of the jet features, we confirm that jets get faster and narrower in winter, but not so clearly in summer, and find no significant trend in jet latitude. Finally, both methods agree on a sudden flow transition in June.

https://doi.org/10.5194/egusphere-2024-3029
Preprint. Discussion started: 8 October 2024

1 Introduction

Extratropical tropopause-level jet streams are narrow bands of westerly winds and are one of the most prominent features of the upper-tropospheric circulation. Their large variability at daily timescales (Woollings et al., 2014) along with their link to extreme weather (e.g., Martius et al., 2006; Mahlstein et al., 2012; Harnik et al., 2014) makes them a prime object of research in meteorology and atmospheric dynamics.

From a climatological perspective, jet streams are often separated into two categories based on their location and momentum source (Kållberg et al., 2005; Koch et al., 2006; Harnik et al., 2014; Winters et al., 2020; Spensberger et al., 2023). The subtropical jet (STJ) is located at the poleward edge of the Hadley cell. It draws its momentum from the thermally-driven Hadley cell circulation and is mostly confined to high levels, typically between 400 and $150\,\mathrm{hPa}$ (Krishnamurti, 1961; Held and Hou, 1980). The eddy-driven jet (EDJ) can be found further poleward, inside the Ferrell cell. It is also referred to as the subpolar or extratropical jet. It is driven by momentum flux convergence associated with midlatitude synoptic eddies (Palmen and Newton, 1948; Held, 1975; Schneider, 1977; Woollings et al., 2010). It has a much deeper vertical extent, typically extending below $700\,\mathrm{hPa}$. The separation into STJ and EDJ is not always clear, both sources of momentum are often present to varying degrees to drive either jets and depend on each other (Lee and Kim, 2003; Martius, 2014).

Certain features and configurations of the jet have received particular attention over the last years due to their links to other aspects of the circulation, surface weather, or both. The latitude of the low-level EDJ has been identified as a major mode of variability of the wintertime Atlantic circulation (Athanasiadis et al., 2010; Woollings et al., 2010; Hannachi et al., 2012). A very zonal (low tilt) EDJ paired with a north-shifted STJ can create a rare but very persistent circulation pattern with a merged jet (Harnik et al., 2014). An instantaneously meandering jet is the marker of Rossby waves (e.g. Vallis, 2017), but strong narrow jets can act as waveguides for them too (Hoskins and Ambrizzi, 1993; Martius et al., 2010; Wirth, 2020; White, 2024). A locally sinuous jet may also mark the presence of a block (e.g. Nakamura and Huang, 2018; Woollings et al., 2018b). Jet properties also interact with each other. For instance, in winter, the EDJ's latitude influences its persistence and predictability (Franzke and Woollings, 2011; Barnes and Hartmann, 2011), and a jet with low speed has a higher daily variability in its waviness and latitude (Woollings et al., 2018a), which is hypothesized to favorise blocks. Jet features have also been linked to extreme events. The position of the EDJ modulates the odds of extreme events in the midlatitudes (Mahlstein et al., 2012), and so does its waviness (Röthlisberger et al., 2016b; Jain and Flannigan, 2021). Over Eurasia, a persistent double jet state is associated with increased odds of extreme heat in summer in certain regions of western Europe (Rousi et al., 2022). Recently, statistical models trained on timeseries of a few (5-10) wintertime EDJ properties (introduced by Barriopedro et al., 2022) were used to skillfully predict air stagnation (Maddison et al., 2023) and temperature extremes (García-Burgos et al., 2023).

Climate change is expected to affect the jet streams in several ways. Through connections highlighted in the previous paragraph, themselves potentially affected by climate change, trends in jet stream properties may translate into trends in various aspects of atmospheric circulation and surface weather (e.g. Held, 1993; Stendel et al., 2021). The poleward shift of the jet streams under climate change was hypothesised very early on (e.g. Held, 1993). It is now observed in historical data in the global mean, albeit more clearly in winter than in summer, and mostly for the EDJ. The signal is however weak in the North

https://doi.org/10.5194/egusphere-2024-3029
Preprint. Discussion started: 8 October 2024

Atlantic sector (Woollings et al., 2023). This poleward shift is projected to continue in future simulations (Barnes and Polvani, 2013; Lachmy, 2022; Woollings et al., 2023). For the STJ, the historical trend is season- and region-dependent. For the North Atlantic sector, Totz et al. (2018) report a poleward trend in the transition seasons and an equatorward trend in summer. The North Atlantic STJ is also weakening with time, especially in summer (Woollings et al., 2023; D'Andrea et al., 2024), and so is the North Atlantic EDJ in the last two decades (Francis and Vavrus, 2012; Woollings et al., 2018a), although an opposite trend has been observed for longer time periods (Blackport and Fyfe, 2022). In future simulations, a positive trend is projected for the maximum speed of the EDJ core, although this signal is not yet apparent in historical data (Shaw and Miyawaki, 2024). In past data and using three different metrics, Francis and Vavrus (2015), Di Capua and Coumou (2016), and Martin (2021) all find slight increases in EDJ waviness, but a stable STJ waviness in the last cited paper. Further downstream however, Lin et al. (2024) find an increase in waviness for the Asian Jet that has an Atlantic origin. By contrast to past trends, for future winters, Peings et al. (2018) find a decrease in waviness accompanied by a strengthening and squeezing of the EDJ. This opposite trend in EDJ waviness for past and future data is consistent with the findings of Cattiaux et al. (2016), who find a slight increase in waviness in the past only for certain basins (including the North Atlantic) and seasons, but an overall decrease in waviness in future simulations. The conflicting results in jet meandering depending on the period and metric chosen were highlighted by Blackport and Screen (2020b) and overall remain a subject of discussion in the community (Geen et al., 2023).

Most of the current research in atmospheric science requires reducing the complexity of the circulation from time-varying 2D or 3D fields to a smaller feature space. These simplified feature spaces are either continuous, like jet indices (Woollings et al., 2010; Di Capua and Coumou, 2016; Barriopedro et al., 2022) or the projection of instantaneous fields on principal components, or discrete, like weather regimes (e.g., Michelangeli et al., 1995) or other types of clustering methods (Weiland et al., 2021; Rousi et al., 2022). These methods can also be categorised based on the number of choices the user needs to make, from data-driven, e.g. principal components, k-means, self-organizing maps, to expert-defined, e.g. jet indices, blocking indices, wave breaking indices. Data-driven approaches are typically less fallible since they require fewer choices, but tend to be harder to interpret than expert-defined features. Data-driven methods are also known to produce physically unrealistic patterns that can lead to wrong interpretations (Monahan and Fyfe, 2006).

In this work and to lay the groundwork for further research on all the interactions previously cited, we develop two complementary diagnostic tools for the jet streams. Using two methods allows us to view the circulation from different angles, and to combine the strengths of data-driven and expert-defined approaches. Recently, Madonna et al. (2017) recommended the use of different, complementary, and problem-dependent approaches to describe the jet streams. Both of the diagnostic tools presented in this work are adaptations of existing techniques widely used in the field of atmospheric sciences, with implementation details changed and tailored for the specific needs of summertime, upper-level circulation.

The first one is a clustering technique known as the self-organizing map (SOM). This data-driven clustering technique creates a distance-preserving discrete feature space that makes it a valuable tool to study stationary and recurrence (Tuel and Martius, 2023), a major factor in extreme events. The second one is a set of jet characteristics computed on individual jet features extracted, tracked, and categorized from wind fields. This provides a collection of continuous interpretable time series representing the jets over time.

https://doi.org/10.5194/egusphere-2024-3029
Preprint. Discussion started: 8 October 2024

After presenting both techniques in detail, we demonstrate their capabilities on reanalysis data. The high-level objectives of the results presented in this work are to assess the seasonal cycle of the upper-level circulation through this new lens, find the trends, or lack thereof, in various metrics, and study to the circulation persistence under different aspects. This works focuses on summer, a season that receives less attention when designing methods to characterize the circulation, and is yet very important for extreme events and which presents interesting, different trends compared to the rest of the year (Harvey et al., 2023).

2 Data and Methods

2.1 Data

The European Centre for Medium-Range Weather Forecasts reanalysis version 5 (hereafter, ERA5 reanalysis; Hersbach et al., 2020) provides 6-hourly gridded fields for the 1959-2022 period, over the $80\,°\mathrm{W} - 40\,°\mathrm{E}$, $15\,°\mathrm{N} - 80\,°\mathrm{N}$ domain. The main variables we use are the horizontal wind components u and v, and the wind speed $U = \sqrt{u^2 + v^2}$, on pressure levels ranging from 175 to $350\,\mathrm{hPa}$.

Both algorithms take as input, at each timestep, a single 2D (longitude-latitude) field of upper-tropospheric wind. We flatten the three wind fields (u, v and U) in the vertical by retaining, at every grid point, their value at the pressure level where U is maximal since the jets are the features that interest us, and they are defined as local wind speed maxima. We keep track, in a separate 2D array, of that pressure level. Both methods then add different preprocessing steps to this flattened data, which will be discussed in the relevant sections.

In addition to wind speed fields, we use $500\,\mathrm{hPa}$ geopoential height anomalies from ERA5, and the daily North Atlantic Oscillation (NAO) index from the United States National Oceanic and Atmospheric Administration, computed following the method developed by Barnston and Livezey (1987) that provides a meaningful definition of NAO in all seasons.

2.2 SOM clustering

2.2.1 Definition

The self-organizing map (SOM) is a clustering method first introduced by Kohonen (1982) (see also Kohonen, 2013, for an in-depth review), whose main appeal over simpler predecessors like k-means is the creation of a 2D distance-preserving discrete feature space. The SOM may be presented as a modification of k-means. In k-means data points are split in k groups called clusters, such that the variance within the clusters is minimal and the variance between clusters is maximal. Each cluster is then represented by the mean of all its members, called the cluster center or sometimes weights matrix. The SOM adds another layer to this algorithm, by arraying the clusters on the nodes of a regular 2D grid of size $k = n \times m$, typically rectangular or hexagonal, based on a distance metric and a neighborhood function. There, a cluster i is defined by its weights matrix $\mathbf{w}_i$ which is not equal in general to its center, but rather the result of a training process during which clusters on neighboring nodes have an influence modulated by the distance between nodes. Hereafter, we conflate the clusters and the nodes they sit on, and

https://doi.org/10.5194/egusphere-2024-3029
Preprint. Discussion started: 8 October 2024

the phrases "distance between clusters" and "neighboring clusters" are to be understood as, respectively, "distance between the nodes on which the clusters sit" and "clusters on neighboring nodes".

The training then has a similar objective as k-means, with the additional constraint that a pair of neighboring clusters should be more similar to each other than a pair of distant clusters. This constraint ensures the distance-preserving property of the created phase space. The desired similarity of neighboring clusters may be enforced by the choice of an appropriate neighborhood function, typically a Gaussian function of the distance between clusters. The convergence is helped by a scale parameter σ that slowly decreases during training, but the decay function and the initial σ value are additional choices that need to be made. In general, a larger σ allows for more similar neighbors, and the limiting case $\sigma \to 0$ is equivalent to k-means.

Both the SOM and k-means share the same challenge, that is the choice of the number of clusters k. The SOM further adds the choice of the shape of the grid, $k = n \times m$. Allowing neighboring clusters to be similar inevitably leads the SOM to be a strictly worse clustering algorithm, in the usual sense of cluster separation, than k-means. It should only be used if one needs a distance-preserving feature space. One of the reasons we use SOM is the interpretability of the projected trajectory. Once the SOM is trained, each timestep belongs to a cluster, its "best matching unit" or BMU, defined as $\mathrm{BMU}(t) = \mathrm{argmin}_i \|\mathbf{x}_t - \mathbf{w}_i\|$. Thus, the input time series is represented as a succession of *stays* in clusters and *jumps* between clusters, where long *stays* or short *jumps* point to persistence, and long *jumps* indicate abrupt changes in the configuration of the upper-level flow.

2.2.2 Specific implementation

For the SOM algorithm, the flattened JJA wind speed field (see Data) is coarsened to a $1.5°$ resolution grid to reduce the computational complexity and to focus on the larger scale features. However, the final results are shown at the initial $0.5°$ resolution. This is done by representing clusters with their centers, computed with the original higher resolution data, rather than their weights.

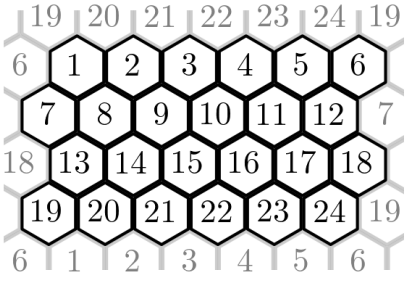

Figure 1. Hexagonal topology SOM with ideal grid size. The SOM clusters are in black and the grayed clusters illustrate the periodic boundaries.

The grid (of size $n \times m$) is hexagonal with periodic boundary conditions, and is associated with a discrete distance metric. All clusters are at a unit distance away from their nearest neighbors, and the bottom row and left column also are at a unit distance away from the top row and right column (see figure 1). In order to inform our decision on the SOM grid size, we use

https://doi.org/10.5194/egusphere-2024-3029
Preprint. Discussion started: 8 October 2024

two performance metrics of the SOM. The first one is the energy function E of the SOM based on Heskes (1999) (see eq. 1), and the second one is the 5$^{\text{th}}$ percentile of the projection of data points on their BMUs, defined as P in eq. 2. These metrics are a function of the ensemble of SOM weights $W = \{\mathbf{w}_i, 1 \leq i \leq n \times m\}$, the ensemble of input data vectors $\mathbf{x} \in X$, of size N, as well as the topological properties of the SOM. The grid distance between two SOM clusters i and j is precomputed and stored in a matric of elements d_{ij}. These distances are then transformed by the neighborhood function to obtain the pairwise neighborhood parameters $h_{ij} = f(d_{ij}; \sigma)$ based on the SOM's scale parameter σ. In this work, f is a zero-mean Gaussian.

$$E(W) = \frac{1}{N} \sum_{\mathbf{x} \in X} \min_{1 \leq i \leq n \times m} \sum_{j=1}^{n \times m} h_{ij} \|\mathbf{x} - \mathbf{w}_j\|^2 \tag{1}$$

$$P(W) = \underset{\mathbf{x} \in X}{Q_5} \left(\max_{1 \leq i \leq n \times m} \frac{\mathbf{x} \cdot \mathbf{w}_i}{\|\mathbf{x}\| \|\mathbf{w}_i\|} \right) \tag{2}$$

The goal is to minimize E and maximize P while maintaining a reasonably low number of clusters. The E and P objectives are similar, but the latter allows one to explicitly limit how poor the poorest projections on the SOM clusters are, making sure that most days are well-described in the 2D feature space described by the SOM since current and future work includes working on extreme configurations of the upper-level circulation. Testing for many sizes ranging from 4×4 to 9×9 was performed, and the chosen size is 6×4.

2.2.3 SOM metrics

We compute statistical properties from the trained SOM, including the populations of each cluster and their annual trends, the average and maximum residence time in a given cluster, and the transition probability matrices at various time lags. Formally, from an integer time series of BMUs $\mathrm{BMU}(t)$, the transition matrix at lag ν (integer number of timesteps forward) M^{ν} has elements $M_{ij}^{\nu} = \mathbb{P}(\mathrm{BMU}(t+\nu) = j | \mathrm{BMU}(t) = i)$.

The transition matrices allow, among other things, to compute a SOM metric that a SOM metric that characterizes immediates predictability in the spririt of the local dimension in dynamical systems theory. Local dimension is a metric that measures, for every point along a high-dimensional trajectory, the amount of active degrees of freedom (see e.g. Faranda et al., 2017). Our predictability metric is named dilution and is defined for each cluster j and lag ν as $\sum_i M_{ij}^{\nu} d_{ij}$. This corresponds to the expected value of d_{ij}, given the discrete probability distribution (for a given cluster j) M_{ij}^{ν}. It informs on how long the SOM-space trajectories leading to cluster i typically are.

The second SOM metric of note is an equivalent to the persistence index in dynamical systems theory. The average (resp. maximum) residence time at a given cluster i is simply given by the average (resp. maximum) length of time during which $\mathrm{BMU}(t) = i$, starting at the transition from another cluster to i. The definition can be loosened to the length of time during which $\mathrm{BMU}(t)$ stays within a given distance of i. With a large SOM with sometimes minute differences between neighboring clusters, this second definition with a small distance of 1 or 2 can be a more realistic measure of persistence. Here, we use a value of 1, meaning a residence on cluster i continues while the trajectory stays on cluster i or any of its six direct neighbors.

https://doi.org/10.5194/egusphere-2024-3029
Preprint. Discussion started: 8 October 2024

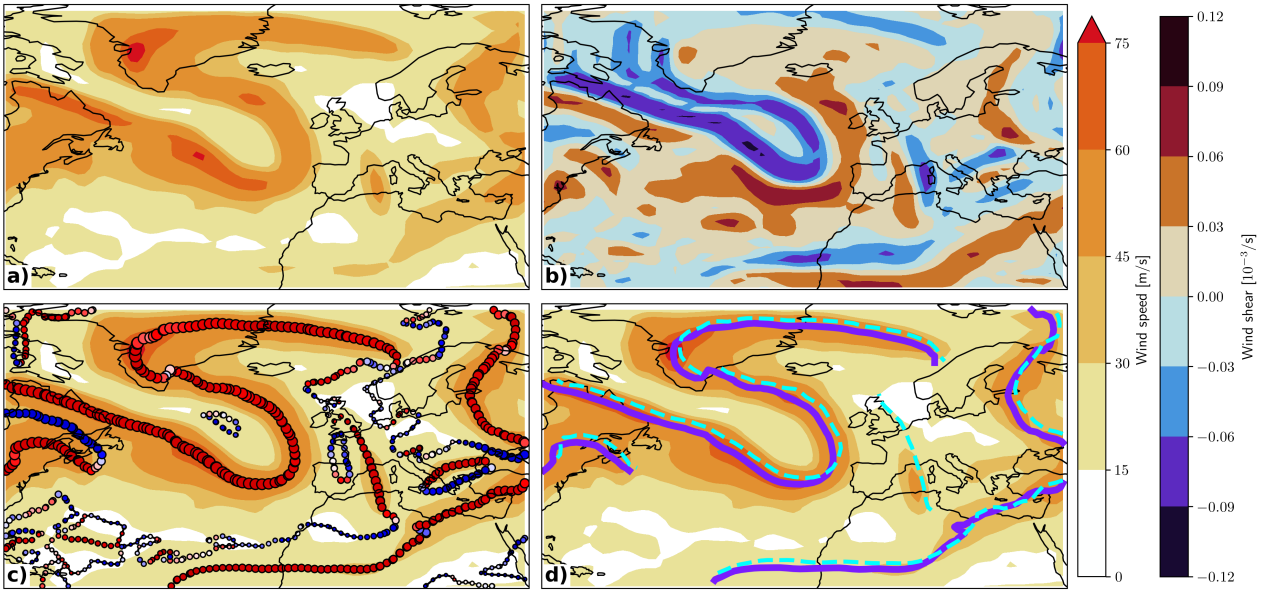

Figure 2. Results of our jet detection algorithm for 0000 UTC 9 Oct 1959. a) The smoothed, flattened wind speed [m/s] field given as input to the algorithm. b) The smoothed horizontal normal wind shear on the same flattened surface. c) The $\tau = 0$ contours where the size of the points corresponds to the wind speed field, and the color corresponds to the alignment with the horizontal wind vector field from blue (close to -1) to red (close to $+1$). d) The jets extracted from contours, as solid purple lines. The output of the S17 algorithm is represented as dashed cyan lines for comparison.

2.3 Feature detection and tracking

The SOM is a powerful data-driven tool to characterize the circulation as a whole in a given region. However, one might want to know more specific information about some of the components of the circulation, expressed as numbers rather than features on a composite map. We now turn to the methods we use to detect jets in flattened 2D wind fields, to separate them into broad categories, to track them over time to assess their lifetime and evolution, and finally to extract a wide range of properties out of them. Thanks to seasonally-varying thresholds (see , our method works equally well across the year. This is why we apply it to the full dataset rather than only to summer, which will allow us to broaden the discussion of inter-annual trends to other seasons and paint a full picture of the summer jets' annual cycles.

2.3.1 Jet detection

Our jet detection algorithm is an updated version of the method by Spensberger et al. (2017, hereafter S17). It can be applied to each timestep independently, allowing for parallelization.

As for the SOM, the flattened wind fields (u, v and U; see Data) are coarsened to a grid of $1.5°$. As a first difference to S17, we use vertical maxima over several high-altitude pressure levels instead of the 2PVU surface. Internal testing has shown

https://doi.org/10.5194/egusphere-2024-3029
Preprint. Discussion started: 8 October 2024

that the STJ is often undetectable on the 2PVU surface in summer, while it clearly appears on our flattened fields. The main criterion used to find jets is the horizontal normal wind shear $\tau := \frac{\partial U}{\partial n} = \frac{v}{U}\frac{\partial U}{\partial x} - \frac{u}{U}\frac{\partial U}{\partial y}$. Following Berry et al. (2007), $\tau = 0$ is a necessary condition for a jet. The first step of this algorithm is thus to find smooth contours of $\tau = 0$. First, a Fourier transform is applied to the τ field in the longitude (λ) and latitude (ϕ) directions, yielding $\tilde{\tau}$ defined on a 2D space of Fourier coefficients (k_λ, k_ϕ). This function is truncated following $|k_\lambda + k_\phi| > K \implies \tilde{\tau}(k_\lambda, k_\phi) = 0$ with $K = 0.3 \times n_\lambda \times n_\phi$ before applying an inverse Fourier transform on the truncated Fourier field. Then, a contour library is applied to extract contours of $\tau = 0$ as lists of (λ, ϕ) coordinate pairs.

Jets are then extracted as subsets of these contours, using wind speed and alignment criteria for each point of the contour. First, the wind speed must be high enough for a grid-point to be considered a part of a potential jet. We use as threshold the day-of-year climatological 75$^{\text{th}}$ percentile of 6-hourly wind speed, so that the algorithm works equally well in all seasons. Second, the contour must be aligned with the wind speed. This is done by computing the local tangent vector $\mathbf{t} = \frac{\mathrm{d}\mathbf{x}}{\mathrm{d}s}$, with s the linear path coordinate, and computing the alignment dot product $a = \frac{\mathbf{t}}{\|\mathbf{t}\|} \cdot \frac{\mathbf{u}}{U}$, as done in Molnos et al. (2017). We require $a > 0.3$ for a jet. With very few values of a different from either -1 or $+1$, the performance of the algorithm is largely insensitive to the exact value of this threshold.

Finally, jets are defined as the longest series of consecutive points that follow these two criteria, allowing for small stretches of 1 to 3 points that do not respect them in between. The jets themselves need to verify two criteria to be considered as such. First, the path integral of the wind speed along their cores needs to be above a day-of-year varying threshold, and the average of all their local alignment dot products needs to be above 0.6.

Each jet J_a of length L_a is represented as a sequence of L_a points $k = 1 \dots L_a$, themselves a collection of coordinates with longitude λ_a^k, latitude ϕ_a^k, pressure p_a^k level, along with additional point-wise properties that can be of use to derive jet properties, e.g. the u_a^k or v_a^k components of wind or the wind speed U_a^k.

Figure 2 demonstrates the jet detection algorithm in four steps and compares its results against the original S17 algorithm. Our algorithm has very comparable results to S17. The two difference, finding 0-contours of τ rather than low values of $\frac{\mathrm{d}\tau U}{\mathrm{d}n}$, and extracting jets as subsets of contours using an alignment criteria instead of connecting points using a shortest-path algorithm, seem to help find jet cores closer to the local wind maxima, a problem that was highlighted in the original work. Furthermore, by allowing jets to not respect the two local criteria (speed and alignment) for up to three points, our algorithm is more likely to find one long jet rather than several shorter pieces. This latter point is sometimes a problem when an EDJ and a STJ are detected as one long single jet. However, this does not happen often in 6-hourly data, and it is typically accompanied by a sudden change in pressure level, wind speed, or alignment along the jet core, which helps to highlight and resolve these cases. This issue is not solved systematically in the current version of the algorithm, but might come in a later version.

2.3.2 Jet properties

Introduced by Woollings et al. (2010), the Jet Latitude Index (JLI) measures the latitude of maximum wind speed in the profile obtained by averaging the wind speed field at low altitudes in a longitudinal band, originally $60\,°\mathrm{W} - 0\,°\mathrm{E}$, the North Atlantic basin. It is often used in combination with the Jet Speed Index (JSI), the maximum wind speed used to find the JLI. These

https://doi.org/10.5194/egusphere-2024-3029
Preprint. Discussion started: 8 October 2024

simple and highly interpretable metrics have been used to describe jet stream variability at timescales ranging from daily to multi-decadal (Woollings et al., 2014, 2018a).

Over time, several other similarly simple yet powerful jet indices have been developed to describe the jet stream in a simplified way, or to link it to other phenomena. Such indices include the zonal jet index (Harnik et al., 2014), several sinuosity/waviness metrics (Francis and Vavrus, 2015; Di Capua and Coumou, 2016; Cattiaux et al., 2016; Röthlisberger et al., 2016a) linked to extreme events and persistence (Röthlisberger et al., 2016b; Martin and Norton, 2023), up to a ten-index toolbox (Barriopedro et al., 2022) that has been used for skillful predictions of cold and hot spells in Europe (Maddison et al., 2023).

In the presence of several jets, many of these indices give an incomplete or improper picture. Using our feature detection algorithm (section 2.3.1), all the jet indices can be computed for each jet object individually. The details of computations and potential differences with the original metrics are explained in the following paragraphs.

In the previous section 2.3.1 we mentioned point-wise jet properties storing each point's position and wind speed. The mean of these point-wise jet properties constitute the first jet properties we compute. The ones of interest correspond to the mean position of the jet. The properties `mean_lon`, `mean_lat` and `mean_lev` are all computed as weighted averages of the longitude λ, the latitude ϕ and the pressure level p respectively, using the point-wise wind speed values U_a^k as weights. In the spirit of the JLI, the maximum wind speed is found and stored as `spe_star`. The position on the (lon-lat) plane of this maximum is stored as `lon_star` and `lat_star`.

A path integral of the wind speed along the jet core and using the haversine distance is performed and stored as `jet_int`. Explicitly, the integral $\int U \mathrm{d}s$ is discretized using central finite differences and computed with a discretized approximation of

$$\mathrm{d}s = 2R \arcsin \sqrt{\sin^2\left(\frac{\mathrm{d}\phi}{2}\right) \cdot \cos^2\left(\frac{\mathrm{d}\lambda}{2}\right) + \cos^2(\phi) \cdot \sin^2\left(\frac{\mathrm{d}\lambda}{2}\right)}$$

with $R = 6.378 \times 10^6\,\mathrm{m}$ the radius of the Earth. This integral is performed once more over a smaller domain ($\lambda > 10\,^\circ\mathrm{W}$) and stored as `int_over_europe`.

To obtain the local width of the jet a at a point k along its core, normal segments are drawn in continuous space on either side of the jet core, of length $10\,^\circ$ each. Along each segment, the wind speed is interpolated from the gridded wind speed field. For each segment, the haversine distance between the core and the first point to have a wind speed below $0.5 \times U_a^k$ represents the local width of the jet on this side, and the full local width is the sum of the local widths computed on either side. In some cases, only one segment can be drawn if the jet core is too close to a boundary. In this case, the local width is simply twice the width computed on the only valid side. The local widths w_a^k are computed only every 5 jet core points to make the computations faster, and then averaged, with U_a^k as weights, to finally obtain the jet's mean `width`.

The tilt of the jet is computed as the slope of a U_a^k-weighted linear fit of the ϕ_a^k against the λ_a^k. The linear coefficient is stored as `tilt`, while the intercept is discarded. The quality of this linear fit, the R^2 value, is used to compute a natural measure of jet waviness: `waviness1` $= 1 - R^2$. Another natural way of characterizing waviness from jet objects is the U_a^k-weighted average distance between ϕ_a^k and `mean_lat`, stored as `waviness2`. For short jets, the difference between the tilt and the waviness is hard to assess, and in this case `waviness1` will not capture waviness well. However, if a jet is both tilted and wavy, only `waviness1` will be able to separate these properties. These two waviness metrics are compared against adaptations

https://doi.org/10.5194/egusphere-2024-3029
Preprint. Discussion started: 8 October 2024

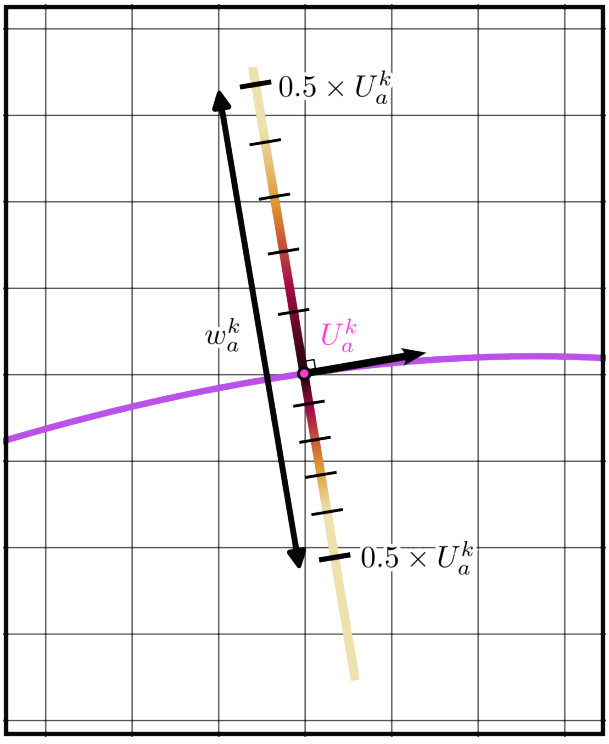

Figure 3. Schematic representing the local width computation, along a jet core a drawn in purple, for a single point k. In the schematic, the wind speed interpolated onto the half-segments is represented using a color gradient from black (core wind speed at the point of interest, U_a^k) to yellow (half of local core wind speed, $0.5 \times U_a^k$) with a tick every $0.1 \times U_a^k$. The schematic, especially the grid spacing, is not to scale.

of waviness metrics found in the recent literature. `wavinessFV15`, adapted from Francis and Vavrus (2015), is computed as the U_a^k-weighted average of the local meridional circulation index: $\mathrm{MCI}_a^k = \frac{(v_a^k - \overline{v_a})|v_a^k|}{(U_a^k)^2}$. `wavinessDC16`, adapted from Di Capua and Coumou (2016), is computed as the ratio between the haversine-integrated length of the jet ($\int 1\mathrm{d}s$) to the length of the circle arc $\overline{\phi} \cdot R \cdot \Delta\lambda_a$, where $\overline{\phi}$ is `mean_lat` and $\Delta\lambda_a$ is the extent of the jet in longitude expressed in radians. Finally, `wavinessR16`, adapted from Röthlisberger et al. (2016a), is computed as the sum of absolute differences in latitudes between neighbors $|\phi_a^{k+1} - \phi_a^k|$, divided by the sum of differences in longitudes.

An index that can be computed that will not be categorized per jet is the double jet index. From the found jets, a 2D (time-lon) binary array is built, where an element is set to `True` if at least 2 jets can be found at this timestep and longitudinal band over all latitudes and one hemisphere. The index is the zonal average of this array for longitudes over Europe, $10\ ^\circ\mathrm{W} < \lambda < 40\ ^\circ\mathrm{E}$.

In section 2.3.4, tracking the jets allows one to add to this list the lifetime of the jet, as well as the instantaneous speed of the jet's center of mass.

https://doi.org/10.5194/egusphere-2024-3029
Preprint. Discussion started: 8 October 2024

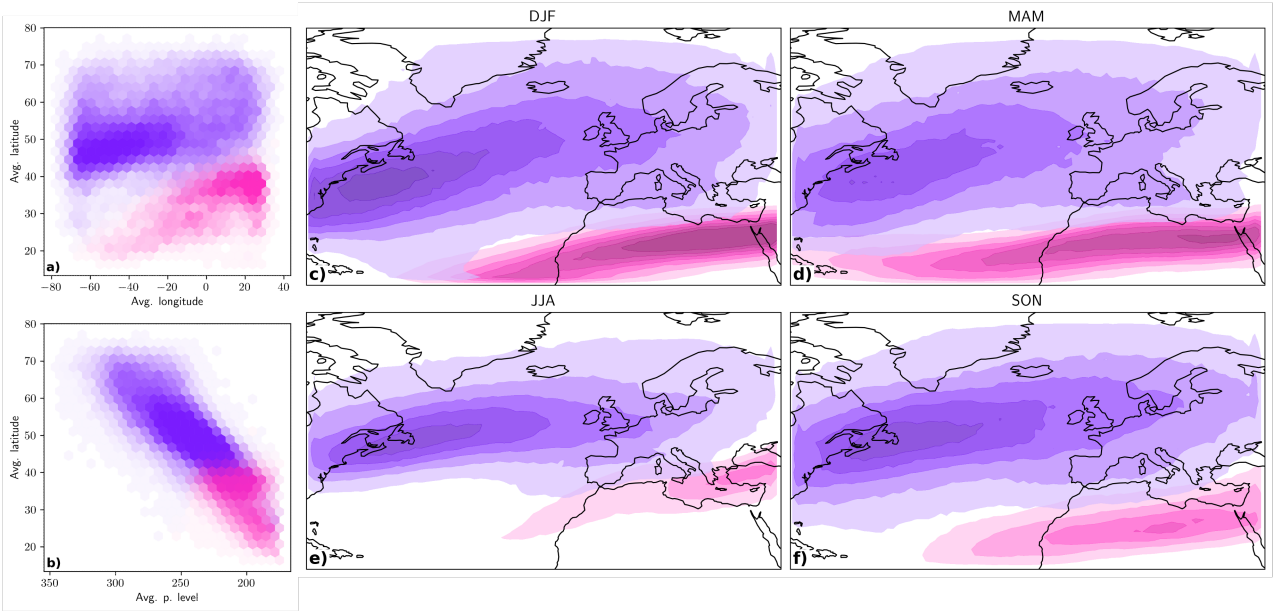

Figure 4. Demonstration of the jet categorization. a, b) For each season, here JJA, the jets are arrayed on the 3D phase space (Mean latitude — Mean longitude — Pressure level) and binned hexagonally. The lightness represents the density of jets in each bin, in arbitrary units. A two-component Gaussian Mixture model is fitted to the projected data, and the labels of each bin are averaged and represented as a color ranging from pink for the STJ to purple for EDJ. c-f) Spatial density of detected jets in arbitrary units, colored by categories: pink for STJ and purple for EDJ for all four seasons. The latter four panels have the same arbitrary scale.

2.3.3 Jet categorization

While some literature sees the types of jets highlighted in the introduction as regimes of a singular jet stream (Harnik et al., 2014, 2016), this framework benefits from seeing them as categories one may assign to the previously detected jets. In instantaneous data, one cannot distinguish the jet from the eddies potentially driving it, since the quantification of the eddy momentum flux requires temporal filtering and averaging (e.g. Lachmy, 2022). One instead has to rely on depth, which is sometimes misleading due to the many factors influencing low-level winds, latitude, which is not sufficient on its own for global data (Winters and Martin, 2017), or potentially other metrics like shear (Martius et al., 2010). A recent, promising approach to establish this categorization bins and counts the jets on the 2D feature space (Wind speed — Potential Temperature). The algorithm then extracts regions of high occurrences for oceanic basins across the world and for both winter and summer. The approach always finds two distinct regions that may be labeled STJ and EDJ, except for the North Atlantic basin in summer (Spensberger et al., 2023, see supplementary material for summer). A very similar approach is used here. It uses the (Mean latitude — Mean longitude — Pressure level) 3D phase space and fits a two-component Gaussian Mixture model to facilitate the discovery of the two regions. The model is fitted independently for each season to accommodate the large seasonal variation in the STJ's mean latitude. Each binned point in the histogram corresponds to a whole jet instead of the jet points used in the original paper.

https://doi.org/10.5194/egusphere-2024-3029
Preprint. Discussion started: 8 October 2024

The demonstration of the jet categorization can be seen on figure 4. Aside from expected results, it shows that the spatial density overlap of the two jets, a potential sign of misdetected jets, is seen mostly over North Africa in winter and is quite low. When studied in more details, most of this spatial overlap is physically sound, as it corresponds to jets of different mean pressure levels, the third dimension of the criterion used, and depths, characterzied using wind speed at low altitude pressure levels (not shown).

2.3.4 Jet tracking

A straightforward feature tracking is presented in this section. The program will assign a flag n to each jet at each timesteps, where the flag is carried over from a jet in a timestep to a jet in the next one according to a distance threshold.

The algorithm starts by assigning each jet in the first timestep a unique flag $1, 2, 3 \ldots$. It then iterates over all timesteps t. For all flags that have appeared at least once in the previous four timesteps ($t-1$, $t-2$, $t-3$, $t-4$, i.e. a day with a time resolution of 6 hours), the algorithm extracts the most recent jet with this flag into a list of potential parents. This allows for jets to disappear for a few timesteps and mitigates the issue of short jets blinking in and out of the jet integral threshold from section 2.3.1. The potential children are all the jets present in the current timestep. For all pair of a potential parent jet a and a child jet b, an overlap measure $o_{a,b}$ as well as a vertical distance $\delta_{a,b}$ are computed as described in equations 3 and 4.

$$o_{a,b} = \frac{|\Lambda_a \cap \Lambda_b|}{2} \left(\frac{1}{L_a} + \frac{1}{L_b} \right) \tag{3}$$

$$\delta_{a,b} = \frac{1}{|\Lambda_a \cap \Lambda_b|} \sum_{k,l:\lambda_k=\lambda_l}^{L_a,L_b} |\phi_l - \phi_l| \tag{4}$$

Where Λ_a is the ensemble of longitudes in jet a.

Both overlap and vertical distance metrics need to satisfy a certain threshold, respectively 0.5 and 10°. If both are met, the jets match and the child jet is assigned the parent's flag. If a child matches no potential parent, it is assigned a new flag, the latest assigned flag plus one. If a child has two potential parents fulfilling both criteria, or if a parent has two children fulfilling them, the winner is the most recent one, and if both are as recent then it is the longest. If the algorithm works on only a portion of the year, the flags are reset at the beginning of each year.

Using this, it is possible to infer the lifetime of a jet from its genesis to its decay, as well as to track the speed of its center of mass (COM), in $\mathrm{m/s}$ using the haversine distance between two 6H-timesteps. The first use of these new jet properties is to filter out jets with 1- or 2-timestep lifetimes to filter out residual noise. The lifetime and COM speed can be seen as additional measures of persistence of the circulation and can be compared against those developed within the framework of the SOM.

https://doi.org/10.5194/egusphere-2024-3029
Preprint. Discussion started: 8 October 2024

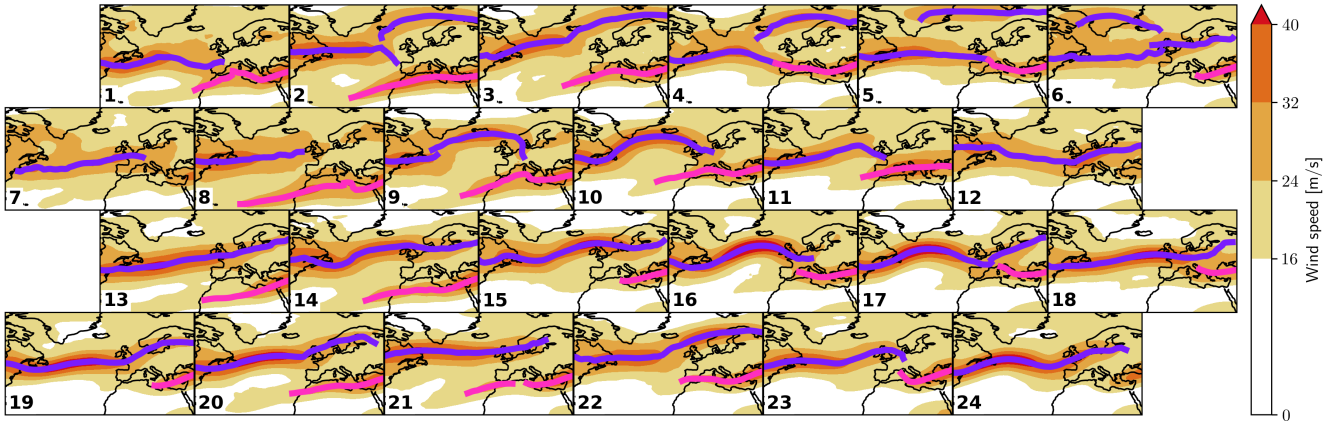

Figure 5. SOM training results on summer wind speed fields. Composites of horizontal wind speed for all days corresponding to a cluster, and result of the jet core detection algorithm overlayed as colored lines; pink for STJ and purple for EDJ. The SOM cluster number is indicated by a number in the bottom left corner.

3 Results

3.1 JJA Atlantic Jet SOM space

The result of the SOM training are summarized in figure 5 on the discrete phase space created by the SOM in a grid that represents its topology. Each panel is a composite of the wind fields of all timesteps belonging to the corresponding cluster. The population of each cluster is shown in Figure 6a). The jet finding and categorization algorithm is applied to these composites, and the results are overlaid with purple and pink lines for the extratropical and STJs, respectively.

The SOM is used with a high number of clusters (24). This is much more than, for example, the canonical four summer weather regimes (Michelangeli et al., 1995; Grams et al., 2017). It allows for a finer separation of timesteps but leads to cluster pairs that look similar at first glance. The interpretation of the SOM can however be simplified, if necessary, by looking at groups of a few clusters at a time, or regions of the phase that exhibit a feature of particular interest. Some of these regions are highlighted here for future reference. It is worth reminding that the boundaries of the SOM space are periodic, meaning that opposite edges form a contiguous region. The high-zonal-overlap double jet states occur on the center-left side, as will be later confirmed when looking at the aggregated jet properties. This region consists of long, south-shifted STJs and large zonal overlaps of the STJ and the EDJ, while the centre right region has shorter or even absent and north-shifted STJs, leading to smaller overlaps. Two clusters (7 and 19) on the left edge have very short STJs, as on the right edge. The jets at the lower left and right edges are at lower latitudes. The EDJ is wavier in the center rows and straighter in the extremal rows. There are a lot of finer scale features in the individual clusters, including some known weather regimes: Scandinavian blocking (clusters 2 and 22), Atlantic ridge (clusters 16 and 17), and Greenland blocking (clusters 6 and 7). This can be supported by looking at geopotential height anomaly composites in Fig. A1 in the Appendix. Some neighboring clusters whose centers look similar

https://doi.org/10.5194/egusphere-2024-3029
Preprint. Discussion started: 8 October 2024

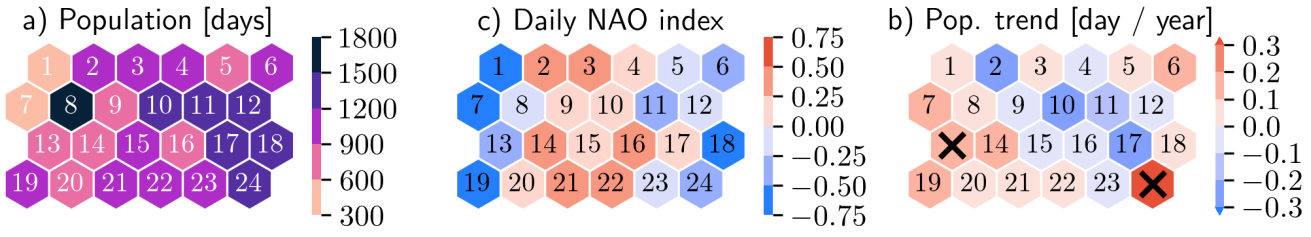

Figure 6. Climatological SOM cluster-wise properties. a) Population, in number of 6-hourly timesteps in JJA 1959 to 2022. b) Daily NAO anomalies averaged over timesteps corresponding to a SOM cluster. No significance testing is done here. c) Trends (1959 - 2022) in population in days per JJA. Significant trends at the 95th percentile are marked with a black cross.

might have differences in intensity or other properties of the jet that are hard to perceive on composite maps, but that will be highlighted when projecting the jet properties onto them in section 3.4.

3.2 SOM statistical properties

Figure 6 shows three SOM cluster-wise properties using a honeycomb grid representing the SOM clusters. The first property is the cluster population. There is up to a factor > 3 between the least and the most visited cluster. The least populated clusters, 1 and 7, both feature shorter southward shifted jets, while the most populated cluster number 8, features both a short EDJ and a long STJ with little overlap over Europe.

The daily NAO index, shown on the second panel b, projects well on the x-axis of the SOM. This shows that the SOM organizes variance in a sensible way, picking up the signal of the main principal component of the circulation variability in the study region. It is, however, not a perfect alignment with the SOM axes, showing that the SOM does more than just discretize the feature space of the first two PCs.

In the third panel c, JJA population trends are shown for all clusters. The most negative trends in population (clusters 2, 10, 17) correspond to, respectively, a Scandinavian blocking, a deep Atlantic ridge with weak jets, and a strong wavy EDJ accompanied by a short and weak STJ with little overlap over eastern Europe. The strongest positive trend, on cluster 24, represents a very similar situation to cluster 17, which showed a negative trend. However, upon closer inspection, it can be observed that the STJ is even weaker and shorter, going below the detection threshold of the jet detection algorithm, and the EDJ is wavier on a shorter wavelength, accompanying geopotential height anomalies in different places over Europe, ultimately resulting vastly different weather situations on the surface. Comparing the trends with the projected NAO indicates an overall weak trend towards more negative NAO and less positive NAO, in accordance to, e.g., Harvey et al. (2023).

The appeal of the SOM in the context of characterizing a complex dynamical system like upper-level Euro-Atlantic circulation is the ability to study high-dimensional time series in a much simpler form; as a series of transitions between clusters separated by long or short stays. The distance-preserving property of the SOM makes the magnitude of the jumps also mean-

https://doi.org/10.5194/egusphere-2024-3029
Preprint. Discussion started: 8 October 2024

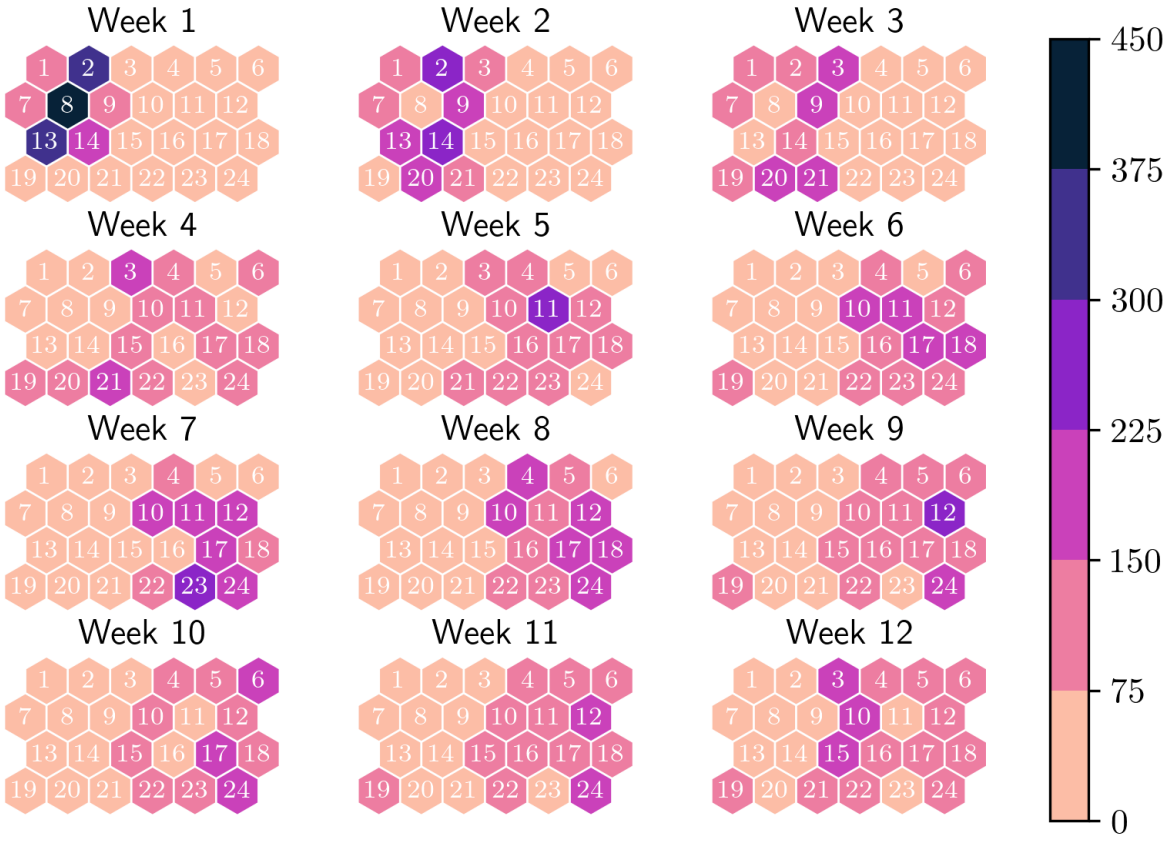

Figure 7. Weekly summer pathway, the weekly-binned cluster population for all weeks of summer and averaged over all summers. Week 1 corresponds to the first week of June and week 12 to the last week of August

ingful, as opposed to other clustering methods. The link back to upper-level flow is easily made by studying the composites in figure 5.

Next we add a temporal dimension by looking at the typical summer pathway through the SOM in figure 7. This figure shows weekly-binned cluster populations for all weeks of JJA and averaged over all summers 1959 to 2022. It shows that the small isolated subset of clusters 2,8,13 corresponds to patterns that represent most of early June's circulation, while the rest of the clusters are visited in July and August, indicating a marked transition of the flow during June. The shift from left to right at the end of June corresponds to a reduction in double jet occurence in JA that will be highlighted in later sections. Cluster 13 corresponds to a negative NAO in early June and cluster 2 to a positive NAO in early June, cluster 8 to an almost neutral NAO state.

https://doi.org/10.5194/egusphere-2024-3029
Preprint. Discussion started: 8 October 2024

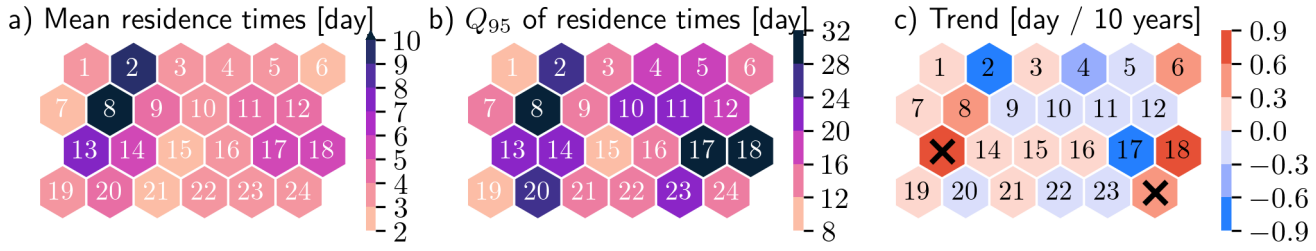

Figure 8. Persistence properties of the SOM clusters. a) Mean residence time. b) 95th percentile of residence times. c) Yearly trend in 95th percentile of residence times in days per decade. Significant trends at the 95th percentile are marked with a black cross. The definition of residence time here is loosened to allow a for a stay to be unbroken as long as the trajectory doesn't leave the radius 1 circle around the starting cluster.

The circulation during these first weeks of June is therefore represented by a few clusters highlighted earlier. The mean error on these clusters is higher than for the rest of the SOM (not shown) so it is safe to assume that they are the default choice for the early June days but not necessarily good representatives.

The nature of the SOM time series makes it a convenient and powerful platform to study crucial features of dynamical systems such as the persistence. In figure 8, the persistence is characterized using the residence time at a cluster, allowing for departures one cluster away from the origin cluster (see methods). The residence times are aggregated as climatological JJA averages (panel a) and the 95th percentile (panel b). The JJA averages give an approximation of the state persistence (Tuel and Martius, 2023), i.e., an estimate of how much time to flow typically needs to move from one state into an next state and the 95th percentiles capture more episodic persistence, i.e., the most persistent events of each flow configuration. Decadal trends in the 95th percentile of residence times are shown in panel c.

Both aggregations (mean and 95th percentile) highlight similar hotspots of high persistence on the top-left and bottom-right corners of the SOM with the exception of cluster 20. However, the high residence times for the clusters in the upper left corner (2,8,13) cannot be interpreted under the same light as the high residence times in clusters 17 and 18. The high residence times in clusters 2,8 and 13 arises from the seasonal pattern, i.e., the circulation resembles theses clusters in early June. The high residence times in clusters 17 and 18 is true state persistence. The most persistent cluster is also the most frequently visited cluster. The least persistent clusters are clusters with a wavy single EDJ, or a short STJ. The clusters with the highest episodic persistence outside the first weeks of June (clusters 17,18, 20 and 23) are quite diverse and fall into neutral (clusters 20, 17, 23) and negative (cluster 18) phases of the NAO, they feature double jets (cluster 20), a straight jet (cluster 18) and wavy jets (clusters 17 and 20).

The trends in residence time follow the trends in population from figure 6. The low number of significant trends and their overall low values suggest that they are probably random.

As residence time can be seen as a discrete-space equivalent to the dynamical system's persistence factor θ^{-1}, a loose equivalent to the local dimension d and a proxy for predictability is found with the backwards dilution. Note that it is not a

https://doi.org/10.5194/egusphere-2024-3029
Preprint. Discussion started: 8 October 2024

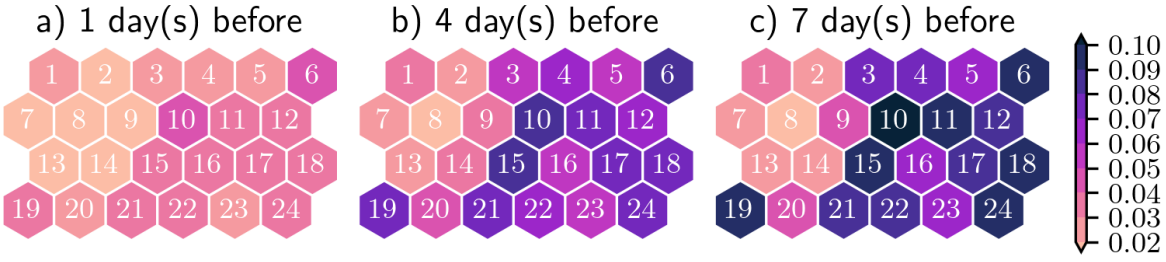

Figure 9. SOM dilution at different backward lags, as defined in methods. A lighter shading on a cluster means that a shorter pathways lead to it.

perfect proxy, as it does not account for the likelihood of transitions. Long jumps, say from cluster 1 to 15, might be very likely in the transition probability matrix, and therefore more predictable, but they would still weigh towards a high backwards dilution of cluster 15. Figure 9 shows that, at a timescale of seven days, shorter pathways lead to the high-overlap double jet states on the top-left than to the lower-overlap or even single jet states. Clusters with the highest dilutions (6 and 10) resemble Greenland blocking, which coincides with the low forecast predictability of this regime (Osman et al., 2023). On the other hand, JA clusters with the lowest backwards dilution resemble the Scandinavian Block and Atlantic Ridge weather regimes. Those results are at odds with the findings of Hochman et al. (2021), who identify a low local dimension anomaly d for Greenland Blocking and a higher d for Scandinavian Block and Atlantic Ridge. This discrepancy either comes from a bad correspondence between backwards dilution and instantaneous local dimension, or the fact we only use JJA data. Some JA clusters with lower dilution also have high persistence (e.g., cluster 20), but not always, for example, clusters 17 and 18 being persistent but unpredictable. This means that while the number of SOM space trajectories leading to these clusters that have length 0 is higher than for other clusters, the rest of them have, on average, high lengths.

3.3 Jet feature properties

From the detected and categorized jets, it is now possible to study the jet feature properties. They are numerous and many of them are correlated with one another, so only a selection of six are shown in the main text, while results for a larger selection of variables are presented Appendix B. The six properties chosen have all seen keen interest in past literature under various forms. The average latitude can be compared to the Jet Latitude Index (Woollings et al., 2010) while the max. speed can be compared to the Jet Speed Index or the 99$^{\text{th}}$ percentile of wind speed (Shaw and Miyawaki, 2024). The speed of the jet's COM can be viewed as a proxy for persistence, the R16 waviness (Röthlisberger et al., 2016b) is one of the most natural way to characterize this property of the detected jet objects, the width of the jet is emerging as another feature of interest in recent literature (Peings et al., 2018) and is here computed using natural coordinates. Finally, we determine, at each longitude, if both jets are present and average this overlap boolean quantity over the European sector ($\lambda > 10\ ^\circ\text{W}$). The mean latitude, max. speed and width's

https://doi.org/10.5194/egusphere-2024-3029
Preprint. Discussion started: 8 October 2024

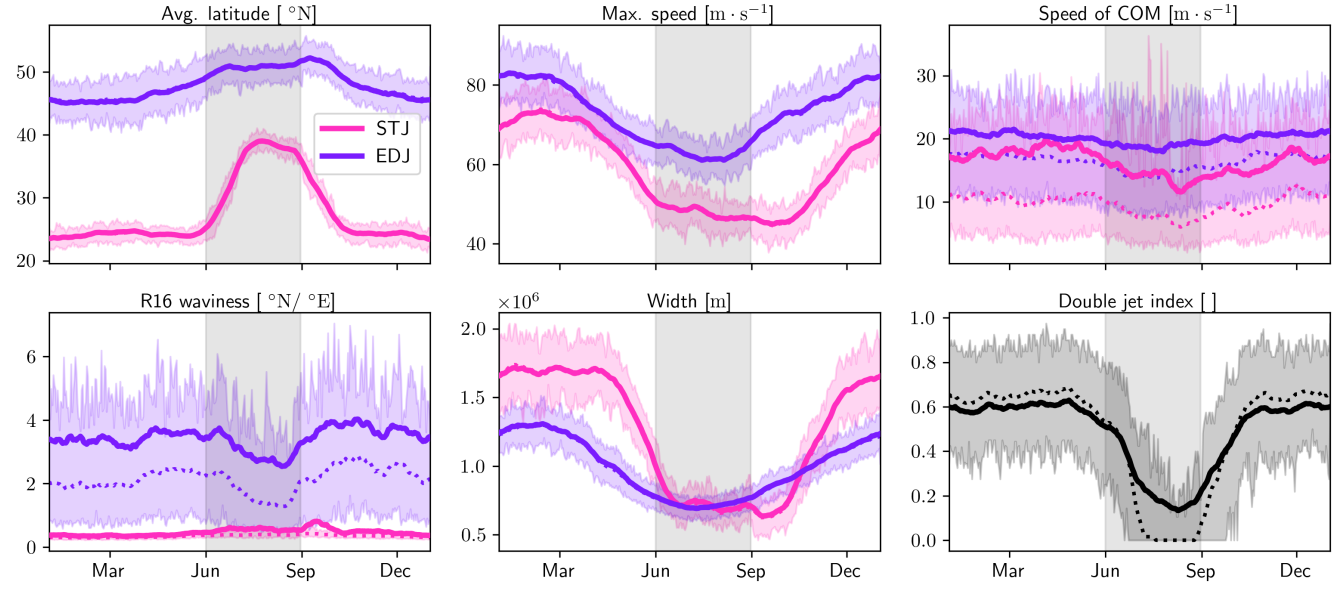

Figure 10. Euro-Atlantic jet properties annual signal, split by jet category. A 15-day-window averaging is applied to the day-of-year mean (thick line) as well as the day-of-year median (thin dotted line) but not to the inter-quartile range (shading). The marker label for each month corresponds to the first day of this month. The grey rectangle in the middle of each panel represents JJA.

distributions have low skew, while the COM speed, waviness and double jet index's distributions are very skewed with tall peaks at low values and long tails.

The yearly cycle of this selection of jet properties is presented in figure 10. All the results are split by jet category and always colored in the same way: pink for the STJ and purple for the EDJ. The double jet index is colored in black. Several interesting features can be observed in this figure. First, the month of June is once more highlighted as a transition month that is different from the rest of summer. More precisely, the speed and width of both jets reduce in the months leading up to June, with a stronger signal for the STJ. Then, during June, both jets move poleward, with again a more pronounced shift for the STJ.

The yearly cycle in latitude and speed of the EDJ are very comparable to the Jet Latitude Index and Jet Speed Index yearly cycles (Woollings et al., 2014) and the storm track yearly cycles (Hoskins and Hodges, 2019) for the equivalent EDJ properties (respectively average latitude and max. speed). The amplitude and width of the summer peak in STJ latitude can be compared with Maher et al. (2020). Seasonally, the STJ follows the expansion and weakening of the Hadley cell in the northern hemisphere summer (Dima and Wallace, 2003; Davis and Rosenlof, 2012), although the relationship between STJ latitude and Hadley cell edge is weakening with global warming (Maher et al., 2020).

The speed of the COM and the R16 waviness do not show strong seasonal cycles in contrast, with signals staying well below the interannual variability, although a dip in STJ COM speed and in EDJ waviness are still noticeable in late summer . Both jets show a clear summer decrease in their widths. The EDJ width is smooth and quasi sinusoidal, while the STJ width jumps from a constant regime to the other in June and October. The jets are much closer together in summer than the rest of the year,

https://doi.org/10.5194/egusphere-2024-3029
Preprint. Discussion started: 8 October 2024

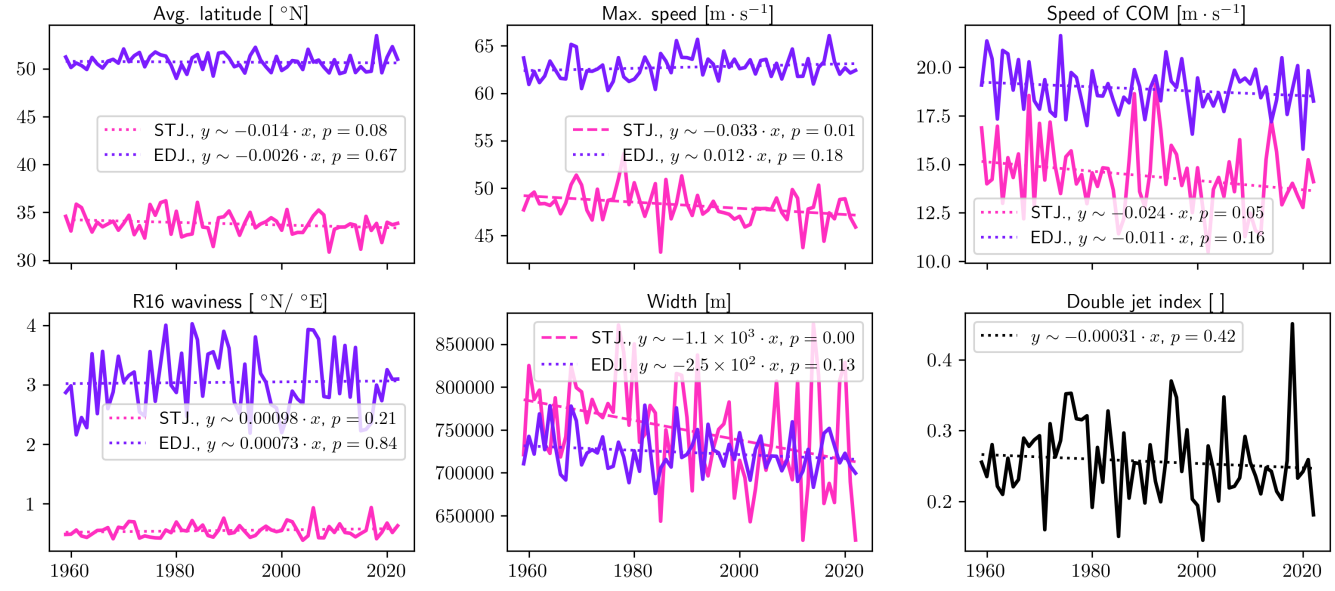

Figure 11. Euro-Atlantic jet properties summer trends, split by jet category. Linear trends represented by dashed lines are significant at the 95$^{\text{th}}$ percentile, while the dotted lines are not.

but overlap less often, mainly due to the subtropical jet occuring less often in summer. This is likely to affect Rossby wave breaking frequency and intensity.

An important questions is how these properties have evolved under the past climate change. Figure 11 shows the JJA trends for the selected six properties, while figure 12 shows the all year trends for the same six properties.

Trends in summer are yet to emerge out of the inter-summer variability, as only two of the eleven trends shown in figure 11 are significant, negative trends in the width and max. speed of the STJ. This STJ speed trend is consistent with the findings of D'Andrea et al. (2024), who report a significant decrease in zonal wind between -0.1 and -0.5 m/s per decade in the area highlighted as the preferred positions of the STJ in summer in figure 4. The trend in STJ width has, to our knowledge, not been explored in the literature. The poleward shift of the EDJ projected in, e.g., Held (1993), is not present in these results in summer, nor is the equatorward trend of the STJ reported by Totz et al. (2018). The absence of a trend in STJ latitude, seemingly at odds with the measured tropical expansion (e.g. Davis and Rosenlof, 2012), is consistent with findings in the recent literature (Davis and Birner, 2017; Maher et al., 2020). The absence of a trend in the persistence proxy for jet objects, the speed in their COM, is in agreement with the small trends in SOM cluster residence times presented earlier. This agreement is to be contrasted with the poor correspondence between state persistence (SOM cluster residence times) and flow persistence (low COM speed) highlighted in section 3.4.

Trends in the annual mean are clearer in contrast, thanks to strong signals in the cold season in particular. Some trends. like for the double jet index, even change signs between summer and all-year. The poleward shift of the EDJ is slow and

https://doi.org/10.5194/egusphere-2024-3029
Preprint. Discussion started: 8 October 2024

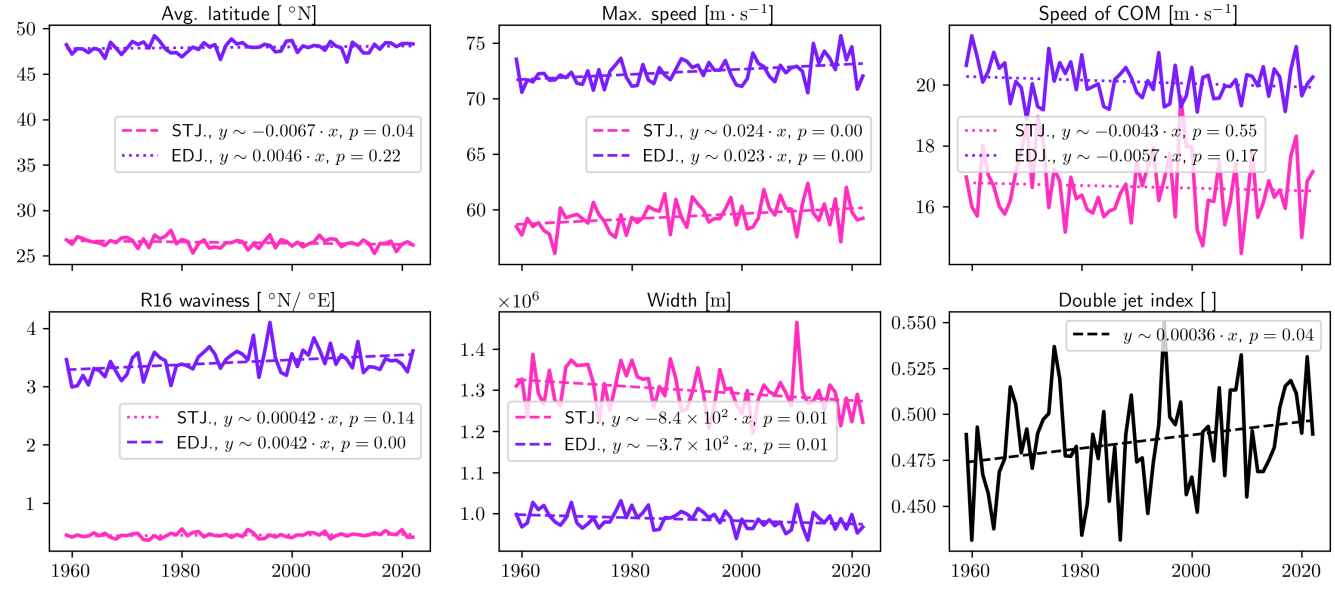

Figure 12. Euro-Atlantic jet properties all-year trends, split by jet category. Linear trends represented by dashed lines are significant at the 95th percentile, while the dotted lines are not.

not significant. Its sign is in accord with Held (1993) and more recent work also studying future simulations (Barnes and Polvani, 2013; Lachmy, 2022). The increase in jet maximum speed is reminiscent of the "fast-get-faster" observation in future simulations by Shaw and Miyawaki (2024) and can also be related to longer-term trends in mean jet speed (Woollings et al., 2018a; Harvey et al., 2023). The slow but significant increase in EDJ waviness over time is not robust to a change of period (see table 1), in accord to findings by Blackport and Screen (2020a). The squeezing of the jet, along with the increase in speed, coincides well with the findings in Peings et al. (2018). The increase in waviness is consistent with Francis and Vavrus (2015), Di Capua and Coumou (2016) and Cattiaux et al. (2016).

More trends of these six jet properties can be viewed in table 1, for the full ERA5 period as well as for a restricted period corresponding to available satellite imaging, 1979-2022, where the reanalysis data is more robust but even more limited in time and in this sense statistically weaker. An extended version of this table with more variables, table B1, can be found in the Appendix. Expectedly, most trends are similar in the two periods, with typically small changes in the value or significance of the trend. It is worth mentioning a few trends that change signs between the two periods, for example the MAM STJ max. speed. Most trends discussed in the previous paragraphs are however valid in both periods, conserving signs and intensities but sometimes losing or gaining significance when computed on the shorter period. Finally, a finer evolution of yearly trends accross seasons can be seen on Appendix figure B1 and shows interesting seasonal shifts in yearly trends, typically around the month of june again. This suggests that the usual seasonal separation that we used on figure 11 and table 1 might not show the full complexity of the seasonally varying trends.

https://doi.org/10.5194/egusphere-2024-3029
Preprint. Discussion started: 8 October 2024

		DJF		MAM		JJA		SON		Year	
		1959-	1979-	1959-	1979-	1959-	1979-	1959-	1979-	1959-	1979-
Avg. latitude	STJ	−1.5	1.5	−7.8	−12	−14	−8.2	7.1	**25**	**−6.7**	0.32
$[10^{-3}\ °\mathrm{N/year}]$	EDJ	8.8	5.9	11	11	−2.6	6.5	0.8	6.4	4.6	7.4
Max. speed	STJ	**3.5**	2.4	1.9	−2.9	**−3.3**	−3.2	**3.4**	**5.6**	**2.4**	0.98
$[10^{-2}\mathrm{m\cdot s^{-1}/year}]$	EDJ	**2.9**	3.8	**2.3**	**6.6**	1.2	−0.12	**2.8**	1.4	**2.3**	**2.9**
R16 waviness	STJ	2.5	1.5	−3.4	**−14**	9.8	−0.42	12	15	4.2	−0.33
$[10^{-4}\ °\mathrm{N}/\ °\mathrm{E/year}]$	EDJ	59	85	23	−95	7.3	−79	**78**	36	**42**	−14
Width	STJ	**−1.8**	−1.6	−0.46	**−2.1**	**−1.1**	−1	**−0.9**	−0.33	**−0.84**	**−1.2**
$[10^{3}\mathrm{m/year}]$	EDJ	**−0.62**	**−1.5**	−0.26	−0.43	−0.25	−0.11	−0.36	−0.52	**−0.37**	**−0.63**
Speed of COM	STJ	−14	7.8	20	−4.9	−24	−17	−14	32	−4.3	6.9
$[10^{-3}\mathrm{m\cdot s^{-1}/year}]$	EDJ	−3.5	7.1	5.9	**23**	−11	2.1	**−14**	−18	−5.7	4
Double jet index $[10^{-4}\ /\mathrm{year}]$		**5.4**	8.2	**13**	**21**	−3.1	−1.2	−0.74	3.6	**3.6**	**7.9**

Table 1. Summary of jet property feature trends for all seasons and the periods 1959-2022 and 1979-2022. Trends are expressed per year and significant trends at the 95$^{\mathrm{th}}$ percentile are written in bold.

3.4 Jet properties on the SOM

As a way to compare and validate the results of both methods, a selection of jet properties are projected onto the SOM clusters, shown in figure 13. The observations made on the latitudinal positions of the jets, as well as the jet overlaps, can all be matched with the jets' mean average latitudes and the mean double jet index. This result is not entirely trivial. It means that, for most clusters, the jets found in the cluster mean wind speed composites have properties corresponding to the mean of the properties of the jets found in each individual timestep belonging to that cluster. In other words, the wind composites and the jets found therein are representative of the wind speed snapshots, as well as their jets, belonging to each cluster and not merely artifacts of averaging noisy fields.

Results from the projection of COM speed seem to indicate that persistence characterized as a slower movement of the jets' COM can hardly be reconciled with the persistence characterized as longer stays on a given SOM cluster, as slow COM speed of either jet are as likely to be associated with long residence times (see again figure 8) as with short ones. This discrepancy is a great motivator for future work on the different facets of this important feature of circulation.

4 Discussion and summary

We use two complementary methods (SOM and jet features) to characterize the upper-level tropospheric jets, and apply them to the Euro-Atlantic sector in the less studied summer season, along with some year-round results. The SOM method specializes

https://doi.org/10.5194/egusphere-2024-3029
Preprint. Discussion started: 8 October 2024

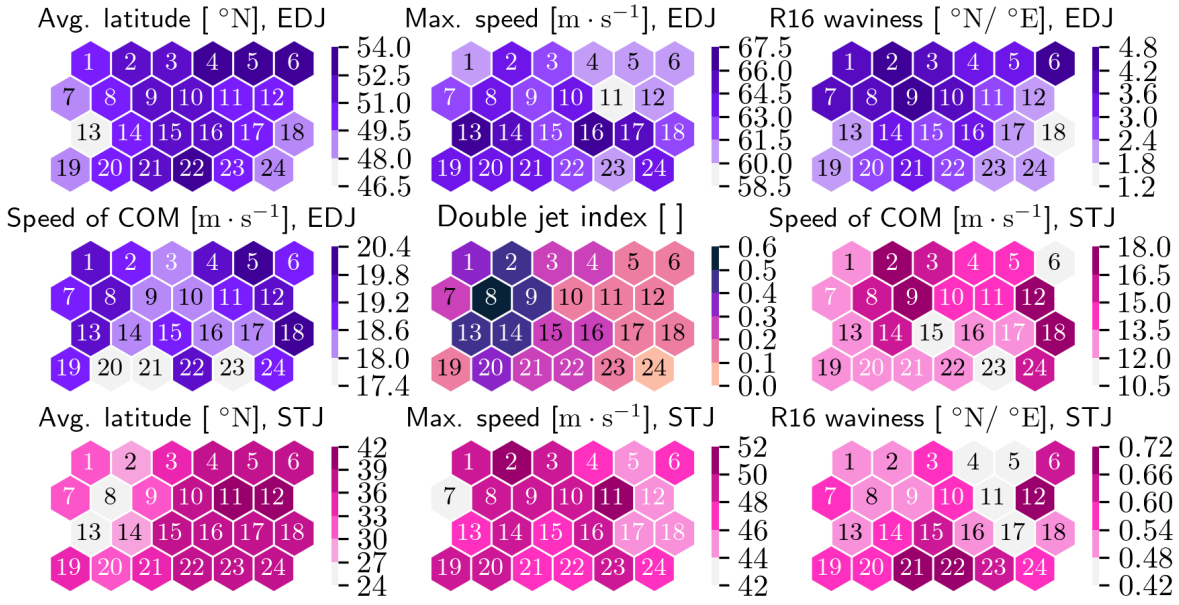

Figure 13. Jet properties, separated by jet category when applicable, projected on the SOM clusters. Shades of purple corresponds to EDJ properties and shades of pink to STJ.

in finding dynamical properties of the overall flow, including persistence and predictability, while the jet features method finds properties of individual jet feature at every timesteps, of which we present trends and seasonal signals. These methods have overlaps, for example the SOM shows a clear seasonal signal in cluster population, and some of the jet feature properties are proxies for persistence. These overlaps allow us to verify the results between methods, increasing our confidence in our results.

The self-organizing map (SOM), a data-driven clustering method with distance-preserving properties, allows us to study the circulation time series as a sequence of stays on a cluster and jumps between clusters, where the magnitude of the jumps is meaningful. This can be directly applied to the evaluation of persistence and predictability. The SOM was able to highlight circulation patterns exhibiting high persistence times, a natural characterization of persistence. The most persistent patterns both correspond to a strong zonal EDJ extending far inland over central Europe and a short STJ over southern Europe. A proxy for predictability on the SOM grid, the backwards dilution, found patterns that are typically reached from neighboring clusters on the SOM rather than far ones. Clusters with low backwards dilution resemble the Scandinavian Block and Atlantic Ridge weather regimes. The SOM was also able to identify the seasonal shift from early to late June, that is confirmed using the jet feature method. Trends in clusters exhibiting certain properties (high overlap of the jets over Europe, blocking) and weekly means of cluster population were also extracted to be compared against the results of the jet feature method showing high consistency. The SOM highlighted known the large scale trend towards more negative NAO in summer, as well as trends in many smaller scale features.

https://doi.org/10.5194/egusphere-2024-3029
Preprint. Discussion started: 8 October 2024

A variation of the jet detection algorithm presented by Spensberger et al. (2017) is used to identify instantaneous jet features and extract per-feature jet properties. The jet features are tracked to obtain metrics offering another view of persistence, and classified into the two canonical jet categories (subtropical and eddy-driven, resp. STJ and EDJ). Once more, past trends and seasonal signals are extracted. In summer, the only significant trends are a decrease of the width and a slowdown of the STJ. This latter trend is consistent with the literature, while the former is, to our knowledge, novel. Over the whole year, we find a significant poleward shift and an increase in waviness of the EDJ, a decrease in width and increase of the maximum speed of both jets, and a decrease of the average latitude of the STJ. The persistence metrics developed around the jet feature method seem to show another facet of persistence to the one expressed by the SOM cluster residence time, and the results of both methods often disagree. However, both methods agree that no aspect of persistence is either increasing or decreasing in time.

Comparing results from the two methods helps to validate them. The subjective jet properties do succeed in characterising features which dominate the leading patterns in the more objective SOM approach. Computing the properties the jet features of every timestep before averaging them based on cluster membership gives very close results to computing jet properties on the jet features extracted from each cluster wind speed composite. This indicates that both methods are coherent with one another. Furthermore, the strong seasonal shift happening in June, characterized most clearly by a weakening and poleward shift of the STJ, is distinctly picked up by both methods.

The jet detection algorithm is directly applicable to global data, as are the jet properties computation and the jet tracking. A global jet categorization would, however, have to use an adapted set of jet properties to distinguish the EDJ from the STJ, as longitude and latitude are only good discriminants in the Atlantic basin. A different set of jet properties might have to be used for each season or even each month, as the seasonal signals suggest. The SOM, like all clustering metrics, is not well suited for a global application and works best when restricted to a single basin. The steep increase in dimensionality and variability that accompanies an expansion to a larger region, combined with the same proportionally small number of timesteps, creates a much more ill-defined clustering problem. Since both methods are relatively cheap computationally, they can be applied to large ensembles and higher-resolution model data to evaluate future trends and shifts in seasonal signal or persistence and predictability properties.

In future work, we will use these diagnostic tools to study the circulation before and during extreme weather events in Europe. Potential applications currently explored include assessing atmospheric persistence and predictability properties in the days leading up heatwaves, finding SOM clusters most likely to see the onset of a damaging hail storm, and discovering which jet properties can be used as good statistical predictors for extreme surface winds.

The previous paragraph pertains to the jet stream as a potential driver of weather predictability, even if the causality can go in both directions. Another use for the methods is the investigation of the drivers of jet stream variability, for example, large-scale teleconnections like ENSO or local mechanisms like diabatic warming, as has been studied recently by Auestad et al. (2024). Another avenue is the exploration of the jets' tight relationship to Rossby waves, for example by assessing the waveguidability of the detected jets (Martius et al., 2010; Wirth, 2020; Bukenberger et al., 2023; White, 2024). Similarly, it is now easier to examine their relationship to Rossby wave breaking, for instance as triggers of large jumps in SOM clusters (Michel and Rivière, 2011), or as drivers for abrupt changes in jet strength, latitude, or center of mass speed (Martius and

https://doi.org/10.5194/egusphere-2024-3029
Preprint. Discussion started: 8 October 2024

Rivière, 2016). Adapting the jet width method to instead find wave breaking events around the jet core is showing promising early results.

Code and data availability. The ERA5 reanalysis data are publicly available at https://cds.climate.copernicus.eu, and the NAO index was downloaded from https://www.cpc.ncep.noaa.gov/products/precip/CWlink/pna/nao.shtml. The package used to obtain the wavebreaking events can be found at https://github.com/skaderli/WaveBreaking, the SOM training and visualization code (honeycomb plots) was adapted from https://github.com/fcomitani/simpsom, and the rest of the code can be found at https://github.com/hbanderier/jetstream_hugo.

https://doi.org/10.5194/egusphere-2024-3029
Preprint. Discussion started: 8 October 2024

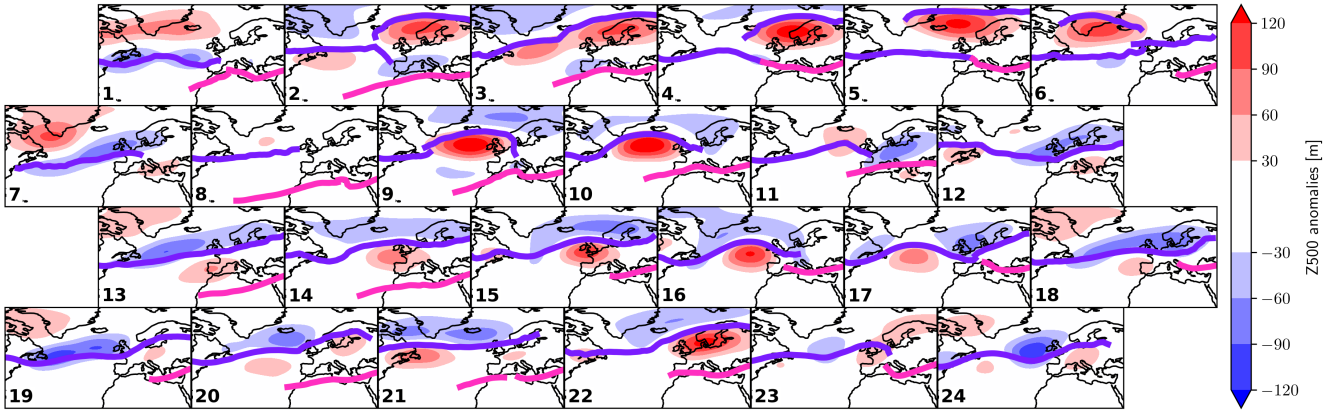

Figure A1. Composites of 500 hPa geopotential height anomaly for all days corresponding to a cluster, and result of the jet core detection algorithm overlayed as colored lines; pink for STJ and purple for EDJ. The SOM cluster number is indicated by a number in the bottom left corner.

Appendix A: More SOM composites

Once the SOM is trained, composites of any other field can be computed by averaging this field over timesteps belonging to each cluster. On Figure A1, we perform this on geopoential height anomalies at 500 hPa to provide more familiar patterns to read and, for example. compare to the usual weather regimes. To remind the reader of the underlying wind fields used to train the SOM, the jet features found in each cluster are overlaid on the composites using the same color code as in the main text. The position of the jets around positive and negative geopotential height anomalies are an indication that the SOM cluster composites seem physically sound and coherent with one another.

Appendix B: Extended jet properties

In the main text, we have highlighted how many jet properties undergo a transition around the month of June, setting this month apart from the rest of summer in terms of absolute values of these jet properties. To explore whether this is also true for the trends explored on, e.g., table 1, we compute, for each calendar day, the yearly trend of each jet property. A 91-day-of-year smoothing is applied to this noisy seasonally-varying trend signal, before it is plotted on Figure B1.

In order to give a more complete overview of the jet properties, we show the seasonal cycle of the complete set on Figure B2, as well as the complete set of yearly trends on table B1.

Comparing the jet core's mean and max speeds shows little difference between the two in their seasonal cycles. The max speed trends are epectedly stronger but they also seem statistically more robust than mean core speed trends. The waviness metrics all show a different seasonal cycle, and even disagree even on which jet category is wavier than the other. Apart from the differences in the original metrics, this discrepancy can also come from how they were adapted to function on jet features,

https://doi.org/10.5194/egusphere-2024-3029
Preprint. Discussion started: 8 October 2024

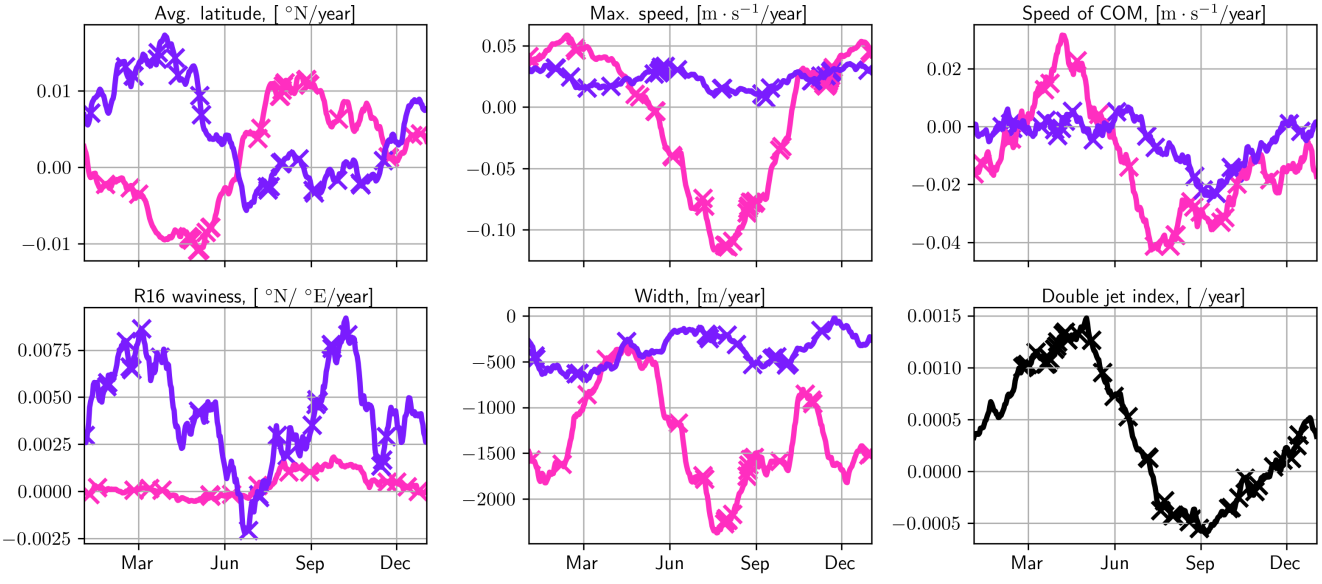

Figure B1. 1959-2022 Day of year yearly trends, smoothed using 91-dayofyear rolling window averaging. Colored crosses indicate a significant trend at the 95th percentile.

and more specifically the normalization factor used in several waviness metrics ($1/\Delta\lambda$) that favorises high values for the STJ which is typically much shorter in this domain. Another issue is that several of these metrics, from their definition, treat tilt (1st derivative) the same way they treat curvature (2nd derivative). FV15 waviness is very close to our definition of tilt, and the seasonal signals of these two metrics are very similar. Naturally, all of the waviness metrics show vastly different trends.

Appendix C: Overview of previously tried methods for feature extraction.

During the development of the jet feature extraction algorithm, several different avenues were explored to improve its robustness or the execution speed and later abandoned in favor of the final version of the algorithm presented in the main text. We believe it is valuable to present negative results, both because these methods could be improved and used again in other relate applications, and simply for future researchers in this field not to try again methods that were explored but ultimately failed at improving the algorithm.

The first version algorithm was an adaptation of the Koch et al. (2006) algorithm, also used in Pena-Ortiz et al. (2013). This algorithm uses a peak finding algorithm on each latitude band, before connecting the points longitudinally based on a distance criterion. The peak finding algorithm requires several thresholds, and their tuning is challenging without an objective quality metric to grade the performance of the algorithm. More fundamentals problem appear with forked jets, like in SOM cluster 2 for instance.

https://doi.org/10.5194/egusphere-2024-3029
Preprint. Discussion started: 8 October 2024

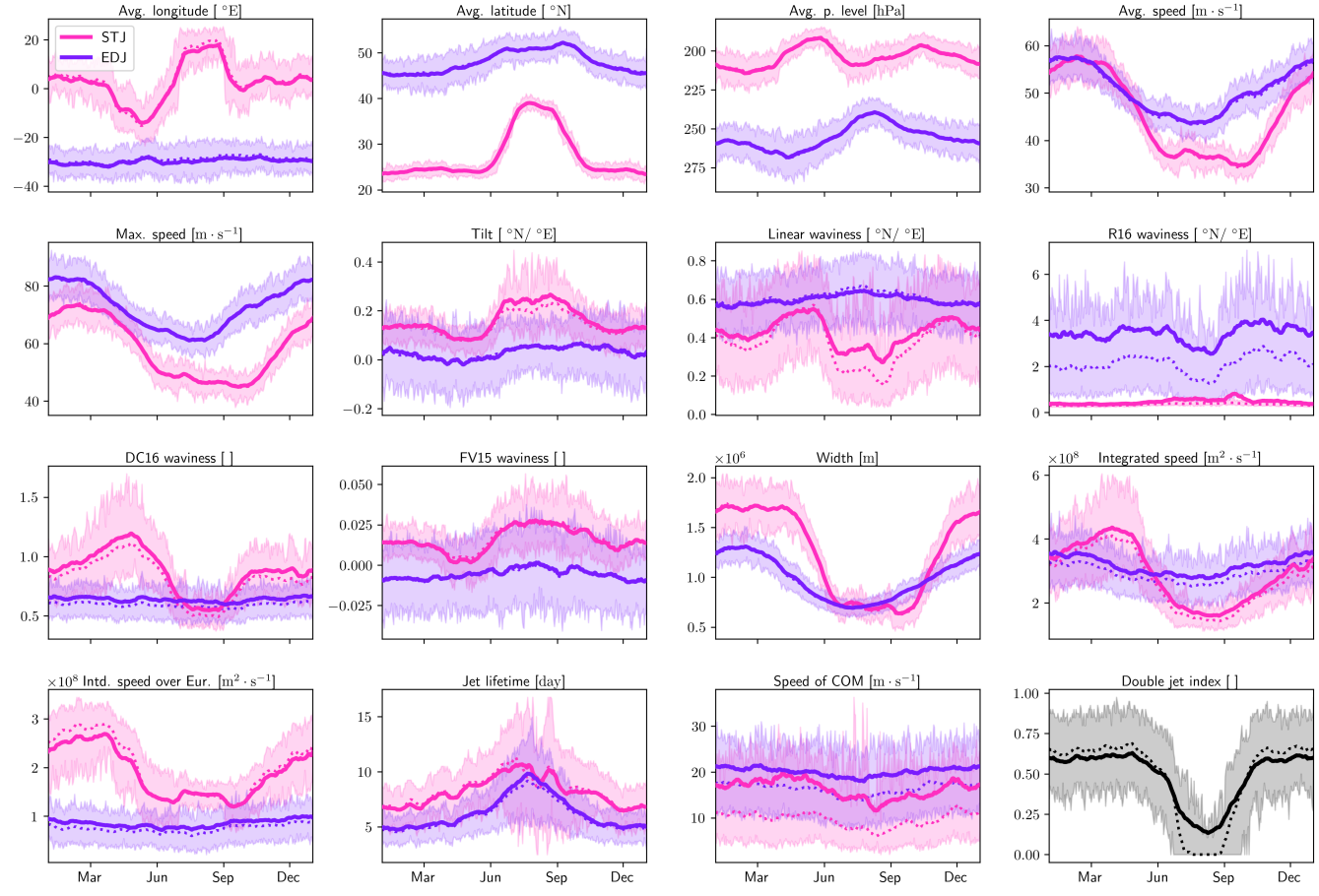

Figure B2. Reproduction of main text's figure 10 with a larger selection of jet properties.

The second version divides the task in two. First, potential jets are found using a fairly low wind speed threshold, that can be made seasonally varying or even a quantile threshold to work well in all seasons. The regions are separated from each other using spatial agglomerative clustering. The second step of the algorithm is heavily inspired by Molnos et al. (2017). From potential jets, the jet cores are found using a weighted shortest path algorithm. Each potential jet region is turned into a graph, with each gridpoint a node and edges connecting all of the nodes. The edges are assigned a weight based on the wind speed of the nodes/grid points it connects, and on its alignment with the directional wind field (similar to the current algorithm).

The difficulty of this second method comes from jet regions connecting to each other if they are too close, and the problem of determining start and end points of jet cores within the jet, with potentially several starts and ends within each potential jet region because of the first problem. Several avenues were explored to mitigate the first problem, which in turn made the second problem easier to solve. Most notably, the use of computed vision techniques like thinning, skeletonization and Sato filtering (Sato et al., 1998). This latter technique is used in medical imaging to highlight vessel like structures in black-and-

https://doi.org/10.5194/egusphere-2024-3029
Preprint. Discussion started: 8 October 2024

white images like blood vessels in biological tissue, and seems very promising to help in jet detection. However, it also requires careful setting of its parameters, most crucially its filtering scales which loosely correspond to the expected width of the jet in pixels. Solving these problems made the algorithm grow in complexity and computing requirements for little added benefits. This approach as well as other related ones were finally abandoned in favor of the simpler, more robust one presented in the main text.

Author contributions. OM and TM outlined the study. HB developed the code and performed the study under the supervision of AT, OM and TM. HB prepared the manuscript with contributions from all co-authors

Competing interests. At least one of the (co-)authors is a member of the editorial board of Weather and Climate Dynamics. The authors have no other competing interests to declare.

Acknowledgements. This work was funded by the Swiss National Science Foundation as part of the project "PERSIST-EUROPE" under grant number 200020_207384.

https://doi.org/10.5194/egusphere-2024-3029
Preprint. Discussion started: 8 October 2024

References

Athanasiadis, P. J., Wallace, J. M., and Wettstein, J. J.: Patterns of Wintertime Jet Stream Variability and Their Relation to the Storm Tracks, https://doi.org/10.1175/2009JAS3270.1, 2010.

Auestad, H., Spensberger, C., Marcheggiani, A., Ceppi, P., Spengler, T., and Woollings, T.: Spatio-Temporal Filtering of Jets Obscures the Reinforcement of Baroclinicity by Latent Heating, https://doi.org/10.5194/egusphere-2024-597, 2024.

Barnes, E. A. and Hartmann, D. L.: Rossby Wave Scales, Propagation, and the Variability of Eddy-Driven Jets, Journal of the Atmospheric Sciences, 68, 2893–2908, https://doi.org/10.1175/JAS-D-11-039.1, 2011.

Barnes, E. A. and Polvani, L.: Response of the Midlatitude Jets, and of Their Variability, to Increased Greenhouse Gases in the CMIP5 Models, Journal of Climate, 26, 7117–7135, https://doi.org/10.1175/JCLI-D-12-00536.1, 2013.

Barnston, A. G. and Livezey, R. E.: Classification, Seasonality and Persistence of Low-Frequency Atmospheric Circulation Patterns, 1987.

Barriopedro, D., Ayarzagüena, B., García-Burgos, M., and García-Herrera, R.: A Multi-Parametric Perspective of the North Atlantic Eddy-Driven Jet, Climate Dynamics, https://doi.org/10.1007/s00382-022-06574-w, 2022.

Berry, G., Thorncroft, C., and Hewson, T.: African Easterly Waves during 2004—Analysis Using Objective Techniques, Monthly Weather Review, 135, 1251–1267, https://doi.org/10.1175/MWR3343.1, 2007.

Blackport, R. and Fyfe: Climate Models Fail to Capture Strengthening Wintertime North Atlantic Jet and Impacts on Europe, https://doi.org/10.1126/sciadv.abn3112, 2022.

Blackport, R. and Screen, J. A.: Insignificant Effect of Arctic Amplification on the Amplitude of Midlatitude Atmospheric Waves, Science Advances, 6, eaay2880, https://doi.org/10.1126/sciadv.aay2880, 2020a.

Blackport, R. and Screen, J. A.: Weakened Evidence for Mid-Latitude Impacts of Arctic Warming, Nature Climate Change, 10, 1065–1066, https://doi.org/10.1038/s41558-020-00954-y, 2020b.

Bukenberger, M., Rüdisühli, S., and Schemm, S.: Jet Stream Dynamics from a Potential Vorticity Gradient Perspective: The Method and Its Application to a Kilometre-Scale Simulation, Quarterly Journal of the Royal Meteorological Society, 149, 2409–2432, https://doi.org/10.1002/qj.4513, 2023.

Cattiaux, J., Peings, Y., Saint-Martin, D., Trou-Kechout, N., and Vavrus, S. J.: Sinuosity of Midlatitude Atmospheric Flow in a Warming World, Geophysical Research Letters, 43, 8259–8268, https://doi.org/10.1002/2016GL070309, 2016.

D'Andrea, F., Duvel, J.-P., Rivière, G., Vautard, R., Cassou, C., Cattiaux, J., Coumou, D., Faranda, D., Happé, T., Jézéquel, A., Ribes, A., and Yiou, P.: Summer Deep Depressions Increase Over the Eastern North Atlantic, Geophysical Research Letters, 51, e2023GL104 435, https://doi.org/10.1029/2023GL104435, 2024.

Davis, N. and Birner, T.: On the Discrepancies in Tropical Belt Expansion between Reanalyses and Climate Models and among Tropical Belt Width Metrics, https://doi.org/10.1175/JCLI-D-16-0371.1, 2017.

Davis, S. M. and Rosenlof, K. H.: A Multidiagnostic Intercomparison of Tropical-Width Time Series Using Reanalyses and Satellite Observations, https://doi.org/10.1175/JCLI-D-11-00127.1, 2012.

Di Capua, G. and Coumou, D.: Changes in Meandering of the Northern Hemisphere Circulation, Environmental Research Letters, 11, 094 028, https://doi.org/10.1088/1748-9326/11/9/094028, 2016.

Dima, I. M. and Wallace, J. M.: On the Seasonality of the Hadley Cell, 2003.

Faranda, D., Messori, G., and Yiou, P.: Dynamical Proxies of North Atlantic Predictability and Extremes, Scientific Reports, 7, 41 278, https://doi.org/10.1038/srep41278, 2017.

https://doi.org/10.5194/egusphere-2024-3029
Preprint. Discussion started: 8 October 2024

Francis, J. A. and Vavrus, S. J.: Evidence Linking Arctic Amplification to Extreme Weather in Mid-Latitudes, Geophysical Research Letters, 39, https://doi.org/10.1029/2012GL051000, 2012.

Francis, J. A. and Vavrus, S. J.: Evidence for a Wavier Jet Stream in Response to Rapid Arctic Warming, Environmental Research Letters, 10, 014 005, https://doi.org/10.1088/1748-9326/10/1/014005, 2015.

Franzke, C. and Woollings, T.: On the Persistence and Predictability Properties of North Atlantic Climate Variability, Journal of Climate, 24, 466–472, https://doi.org/10.1175/2010JCLI3739.1, 2011.

García-Burgos, M., Ayarzagüena, B., Barriopedro, D., and García-Herrera, R.: Jet Configurations Leading to Extreme Winter Temperatures Over Europe, Journal of Geophysical Research: Atmospheres, 128, e2023JD039 304, https://doi.org/10.1029/2023JD039304, 2023.

Geen, R., Thomson, S. I., Screen, J. A., Blackport, R., Lewis, N. T., Mudhar, R., Seviour, W. J. M., and Vallis, G. K.: An Explanation for the Metric Dependence of the Midlatitude Jet-Waviness Change in Response to Polar Warming, Geophysical Research Letters, 50, e2023GL105 132, https://doi.org/10.1029/2023GL105132, 2023.

Grams, C. M., Beerli, R., Pfenninger, S., Staffell, I., and Wernli, H.: Balancing Europe's Wind-Power Output through Spatial Deployment Informed by Weather Regimes, Nature Climate Change, 7, 557–562, https://doi.org/10.1038/nclimate3338, 2017.

Hannachi, A., Woollings, T., and Fraedrich, K.: The North Atlantic Jet Stream: A Look at Preferred Positions, Paths and Transitions, Quarterly Journal of the Royal Meteorological Society, 138, 862–877, https://doi.org/10.1002/qj.959, 2012.

Harnik, N., Galanti, E., Martius, O., and Adam, O.: The Anomalous Merging of the African and North Atlantic Jet Streams during the Northern Hemisphere Winter of 2010, Journal of Climate, 27, 7319–7334, https://doi.org/10.1175/JCLI-D-13-00531.1, 2014.

Harnik, N., Garfinkel, C. I., and Lachmy, O.: The Influence of Jet Stream Regime on Extreme Weather Events, in: Dynamics and Predictability of Large-Scale, High-Impact Weather and Climate Events, edited by Li, J., Swinbank, R., Grotjahn, R., and Volkert, H., pp. 79–94, Cambridge University Press, 1 edn., ISBN 978-1-107-77554-1 978-1-107-07142-1 978-1-107-41680-2, https://doi.org/10.1017/CBO9781107775541.007, 2016.

Harvey, B., Hawkins, E., and Sutton, R.: Storylines for Future Changes of the North Atlantic Jet and Associated Impacts on the UK, International Journal of Climatology, 43, 4424–4441, https://doi.org/10.1002/joc.8095, 2023.

Held, I. M.: Momentum Transport by Quasi-Geostrophic Eddies, Journal of the Atmospheric Sciences, 32, 1494–1497, https://doi.org/10.1175/1520-0469(1975)032<1494:MTBQGE>2.0.CO;2, 1975.

Held, I. M.: Large-Scale Dynamics and Global Warming, Bulletin of the American Meteorological Society, 74, 228–242, https://doi.org/10.1175/1520-0477(1993)074<0228:LSDAGW>2.0.CO;2, 1993.

Held, I. M. and Hou, A. Y.: Nonlinear Axially Symmetric Circulations in a Nearly Inviscid Atmosphere, Journal of the Atmospheric Sciences, 37, 515–533, https://doi.org/10.1175/1520-0469(1980)037<0515:NASCIA>2.0.CO;2, 1980.

Hersbach, H., Bell, B., Berrisford, P., Hirahara, S., Horányi, A., Muñoz-Sabater, J., Nicolas, J., Peubey, C., Radu, R., Schepers, D., Simmons, A., Soci, C., Abdalla, S., Abellan, X., Balsamo, G., Bechtold, P., Biavati, G., Bidlot, J., Bonavita, M., De Chiara, G., Dahlgren, P., Dee, D., Diamantakis, M., Dragani, R., Flemming, J., Forbes, R., Fuentes, M., Geer, A., Haimberger, L., Healy, S., Hogan, R. J., Hólm, E., Janisková, M., Keeley, S., Laloyaux, P., Lopez, P., Lupu, C., Radnoti, G., de Rosnay, P., Rozum, I., Vamborg, F., Villaume, S., and Thépaut, J.-N.: The ERA5 Global Reanalysis, Quarterly Journal of the Royal Meteorological Society, 146, 1999–2049, https://doi.org/10.1002/qj.3803, 2020.

Heskes, T.: Energy Functions for Self-Organizing Maps, in: Kohonen Maps, edited by Oja, E. and Kaski, S., pp. 303–315, Elsevier Science B.V., Amsterdam, ISBN 978-0-444-50270-4, https://doi.org/10.1016/B978-044450270-4/50024-3, 1999.

https://doi.org/10.5194/egusphere-2024-3029
Preprint. Discussion started: 8 October 2024

Hochman, A., Messori, G., Quinting, J. F., Pinto, J. G., and Grams, C. M.: Do Atlantic-European Weather Regimes Physically Exist?, Geophysical Research Letters, 48, e2021GL095 574, https://doi.org/10.1029/2021GL095574, 2021.

Hoskins, B. J. and Ambrizzi, T.: Rossby Wave Propagation on a Realistic Longitudinally Varying Flow, 1993.

Hoskins, B. J. and Hodges, K. I.: The Annual Cycle of Northern Hemisphere Storm Tracks. Part II: Regional Detail, Journal of Climate, 32, 1761–1775, https://doi.org/10.1175/JCLI-D-17-0871.1, 2019.

Jain, P. and Flannigan, M.: The Relationship between the Polar Jet Stream and Extreme Wildfire Events in North America, Journal of Climate, 34, 6247–6265, https://doi.org/10.1175/JCLI-D-20-0863.1, 2021.

Kållberg, P., Berrisford, P., Hoskins, B., Simmons, A., Uppala, S., Lamy-Thépaut, S., and Hine, R.: ERA-40 Atlas, Tech. Rep. 19, ECMWF, 2005.

Koch, P., Wernli, H., and Davies, H. C.: An Event-Based Jet-Stream Climatology and Typology, International Journal of Climatology, 26, 283–301, https://doi.org/10.1002/joc.1255, 2006.

Kohonen, T.: Self-Organized Formation of Topologically Correct Feature Maps, Biological Cybernetics, 43, 59–69, https://doi.org/10.1007/BF00337288, 1982.

Kohonen, T.: Essentials of the Self-Organizing Map, Neural Networks, 37, 52–65, https://doi.org/10.1016/j.neunet.2012.09.018, 2013.

Krishnamurti, T. N.: The Subtropical Jets Stream of Winter, Journal of the Atmospheric Sciences, 18, 172–191, https://doi.org/10.1175/1520-0469(1961)018<0172:TSJSOW>2.0.CO;2, 1961.

Lachmy, O.: The Relation Between the Latitudinal Shifts of Midlatitude Diabatic Heating, Eddy Heat Flux, and the Eddy-Driven Jet in CMIP6 Models, Journal of Geophysical Research: Atmospheres, 127, https://doi.org/10.1029/2022JD036556, 2022.

Lee, S. and Kim, H.-k.: The Dynamical Relationship between Subtropical and Eddy-Driven Jets, Journal of the Atmospheric Sciences, 60, 1490–1503, https://doi.org/10.1175/1520-0469(2003)060<1490:TDRBSA>2.0.CO;2, 2003.

Lin, L., Hu, C., Wang, B., Wu, R., Wu, Z., Yang, S., Cai, W., Li, P., Xiong, X., and Chen, D.: Atlantic Origin of the Increasing Asian Westerly Jet Interannual Variability, Nature Communications, 15, 2155, https://doi.org/10.1038/s41467-024-46543-x, 2024.

Maddison, J. W., Ayarzagüena, B., Barriopedro, D., and García-Herrera, R.: Added Value of a Multiparametric Eddy-Driven Jet Diagnostic for Understanding European Air Stagnation, Environmental Research Letters, 18, 084 022, https://doi.org/10.1088/1748-9326/ace72e, 2023.

Madonna, E., Li, C., Grams, C. M., and Woollings, T.: The Link between Eddy-Driven Jet Variability and Weather Regimes in the North Atlantic-European Sector, Quarterly Journal of the Royal Meteorological Society, 143, 2960–2972, https://doi.org/10.1002/qj.3155, 2017.

Maher, P., Kelleher, M. E., Sansom, P. G., and Methven, J.: Is the Subtropical Jet Shifting Poleward?, Climate Dynamics, 54, 1741–1759, https://doi.org/10.1007/s00382-019-05084-6, 2020.

Mahlstein, I., Martius, O., Chevalier, C., and Ginsbourger, D.: Changes in the Odds of Extreme Events in the Atlantic Basin Depending on the Position of the Extratropical Jet, Geophysical Research Letters, 39, https://doi.org/10.1029/2012GL053993, 2012.

Martin, J. E.: Recent Trends in the Waviness of the Northern Hemisphere Wintertime Polar and Subtropical Jets, Journal of Geophysical Research: Atmospheres, 126, e2020JD033 668, https://doi.org/10.1029/2020JD033668, 2021.

Martin, J. E. and Norton, T.: Waviness of the Southern Hemisphere Wintertime Polar and Subtropical Jets, Weather and Climate Dynamics, 4, 875–886, https://doi.org/10.5194/wcd-4-875-2023, 2023.

Martius, O.: A Lagrangian Analysis of the Northern Hemisphere Subtropical Jet, https://doi.org/10.1175/JAS-D-13-0329.1, 2014.

Martius, O. and Rivière, G.: Rossby Wave Breaking: Climatology, Interaction with Low-Frequency Climate Variability, and Links to Extreme Weather Events, in: Dynamics and Predictability of Large-Scale, High-Impact Weather and Climate Events, edited by Li, J., Swinbank,

https://doi.org/10.5194/egusphere-2024-3029
Preprint. Discussion started: 8 October 2024

R., Grotjahn, R., and Volkert, H., pp. 69–78, Cambridge University Press, 1 edn., ISBN 978-1-107-77554-1 978-1-107-07142-1 978-1-107-41680-2, https://doi.org/10.1017/CBO9781107775541.006, 2016.

Martius, O., Zenklusen, E., Schwierz, C., and Davies, H. C.: Episodes of Alpine Heavy Precipitation with an Overlying Elongated Stratospheric Intrusion: A Climatology, International Journal of Climatology, 26, 1149–1164, https://doi.org/10.1002/joc.1295, 2006.

Martius, O., Schwierz, C., and Davies, H. C.: Tropopause-Level Waveguides, Journal of the Atmospheric Sciences, 67, 866–879, https://doi.org/10.1175/2009JAS2995.1, 2010.

Michel, C. and Rivière, G.: The Link between Rossby Wave Breakings and Weather Regime Transitions, Journal of the Atmospheric Sciences, 68, 1730–1748, https://doi.org/10.1175/2011JAS3635.1, 2011.

Michelangeli, P.-A., Vautard, R., and Legras, B.: Weather Regimes: Recurrence and Quasi Stationarity, Journal of the Atmospheric Sciences, 52, 1237–1256, https://doi.org/10.1175/1520-0469(1995)052<1237:WRRAQS>2.0.CO;2, 1995.

Molnos, S., Mamdouh, T., Petri, S., Nocke, T., Weinkauf, T., and Coumou, D.: A Network-Based Detection Scheme for the Jet Stream Core, Earth System Dynamics, 8, 75–89, https://doi.org/10.5194/esd-8-75-2017, 2017.

Monahan, A. H. and Fyfe, J. C.: On the Nature of Zonal Jet EOFs, https://doi.org/10.1175/JCLI3960.1, 2006.

Nakamura, N. and Huang, C. S. Y.: Atmospheric Blocking as a Traffic Jam in the Jet Stream, Science, 361, 42–47, https://doi.org/10.1126/science.aat0721, 2018.

Osman, M., Beerli, R., Büeler, D., and Grams, C. M.: Multi-Model Assessment of Sub-Seasonal Predictive Skill for Year-Round Atlantic–European Weather Regimes, Quarterly Journal of the Royal Meteorological Society, 149, 2386–2408, https://doi.org/10.1002/qj.4512, 2023.

Palmen, E. and Newton, C. W.: A Study of the Mean Wind and Temperature Distribution in the Vicinity of the Polar Front in Winter, Journal of the Atmospheric Sciences, 5, 220–226, https://doi.org/10.1175/1520-0469(1948)005<0220:ASOTMW>2.0.CO;2, 1948.

Peings, Y., Cattiaux, J., Vavrus, S. J., and Magnusdottir, G.: Projected Squeezing of the Wintertime North-Atlantic Jet, Environmental Research Letters, 13, 074 016, https://doi.org/10.1088/1748-9326/aacc79, 2018.

Pena-Ortiz, C., Gallego, D., Ribera, P., Ordonez, P., and Alvarez-Castro, M. D. C.: Observed Trends in the Global Jet Stream Characteristics during the Second Half of the 20th Century, Journal of Geophysical Research: Atmospheres, 118, 2702–2713, https://doi.org/10.1002/jgrd.50305, 2013.

Röthlisberger, M., Martius, O., and Wernli, H.: An Algorithm for Identifying the Initiation of Synoptic-Scale Rossby Waves on Potential Vorticity Waveguides, Quarterly Journal of the Royal Meteorological Society, 142, 889–900, https://doi.org/10.1002/qj.2690, 2016a.

Röthlisberger, M., Pfahl, S., and Martius, O.: Regional-Scale Jet Waviness Modulates the Occurrence of Midlatitude Weather Extremes: JET WAVINESS AND WEATHER EXTREMES, Geophysical Research Letters, 43, 10,989–10,997, https://doi.org/10.1002/2016GL070944, 2016b.

Rousi, E., Kornhuber, K., Beobide-Arsuaga, G., Luo, F., and Coumou, D.: Accelerated Western European Heatwave Trends Linked to More-Persistent Double Jets over Eurasia, Nature Communications, 13, 3851, https://doi.org/10.1038/s41467-022-31432-y, 2022.

Sato, Y., Nakajima, S., Shiraga, N., Atsumi, H., Yoshida, S., Koller, T., Gerig, G., and Kikinis, R.: Three-Dimensional Multi-Scale Line Filter for Segmentation and Visualization of Curvilinear Structures in Medical Images, Medical Image Analysis, 2, 143–168, https://doi.org/10.1016/s1361-8415(98)80009-1, 1998.

Schneider, E. K.: Axially Symmetric Steady-State Models of the Basic State for Instability and Climate Studies. Part II. Nonlinear Calculations, Journal of the Atmospheric Sciences, 34, 280–296, https://doi.org/10.1175/1520-0469(1977)034<0280:ASSSMO>2.0.CO;2, 1977.

https://doi.org/10.5194/egusphere-2024-3029
Preprint. Discussion started: 8 October 2024

Shaw, T. A. and Miyawaki, O.: Fast Upper-Level Jet Stream Winds Get Faster under Climate Change, Nature Climate Change, 14, 61–67, https://doi.org/10.1038/s41558-023-01884-1, 2024.

Spensberger, C., Spengler, T., and Li, C.: Upper-Tropospheric Jet Axis Detection and Application to the Boreal Winter 2013/14, Monthly Weather Review, 145, 2363–2374, https://doi.org/10.1175/MWR-D-16-0467.1, 2017.

Spensberger, C., Li, C., and Spengler, T.: Linking Instantaneous and Climatological Perspectives on Eddy-Driven and Subtropical Jets, Journal of Climate, 36, 8525–8537, https://doi.org/10.1175/JCLI-D-23-0080.1, 2023.

Stendel, M., Francis, J., White, R., Williams, P. D., and Woollings, T.: The Jet Stream and Climate Change, in: Climate Change, pp. 327–357, Elsevier, ISBN 978-0-12-821575-3, https://doi.org/10.1016/B978-0-12-821575-3.00015-3, 2021.

Totz, S., Petri, S., Lehmann, J., and Coumou, D.: Regional Changes in the Mean Position and Variability of the Tropical Edge, Geophysical Research Letters, 45, 12,076–12,084, https://doi.org/10.1029/2018GL079911, 2018.

Tuel, A. and Martius, O.: Weather Persistence on Sub-Seasonal to Seasonal Timescales: A Methodological Review, Preprint, Dynamics of the Earth system: concepts, https://doi.org/10.5194/egusphere-2023-111, 2023.

Vallis, G. K.: Atmospheric and Oceanic Fluid Dynamics: Fundamentals and Large-Scale Circulation, Cambridge University Press, 2 edn., ISBN 978-1-107-06550-5 978-1-107-58841-7, https://doi.org/10.1017/9781107588417, 2017.

Weiland, R. S., van der Wiel, K., Selten, F., and Coumou, D.: Intransitive Atmosphere Dynamics Leading to Persistent Hot–Dry or Cold–Wet European Summers, Journal of Climate, 34, 6303–6317, https://doi.org/10.1175/JCLI-D-20-0943.1, 2021.

White, R. H.: Time-Varying Atmospheric Waveguides – Climatologies and Connections to Quasi-Stationary Waves, EGUsphere, pp. 1–21, https://doi.org/10.5194/egusphere-2024-966, 2024.

Winters, A. C. and Martin, J. E.: Diagnosis of a North American Polar–Subtropical Jet Superposition Employing Piecewise Potential Vorticity Inversion, Monthly Weather Review, 145, 1853–1873, https://doi.org/10.1175/MWR-D-16-0262.1, 2017.

Winters, A. C., Keyser, D., Bosart, L. F., and Martin, J. E.: Composite Synoptic-Scale Environments Conducive to North American Polar–Subtropical Jet Superposition Events, Monthly Weather Review, 148, 1987–2008, https://doi.org/10.1175/MWR-D-19-0353.1, 2020.

Wirth, V.: Waveguidability of Idealized Midlatitude Jets and the Limitations of Ray Tracing Theory, Weather and Climate Dynamics, 1, 111–125, https://doi.org/10.5194/wcd-1-111-2020, 2020.

Woollings, T., Hannachi, A., and Hoskins, B.: Variability of the North Atlantic Eddy-Driven Jet Stream: Variability of the North Atlantic Jet Stream, Quarterly Journal of the Royal Meteorological Society, 136, 856–868, https://doi.org/10.1002/qj.625, 2010.

Woollings, T., Czuchnicki, C., and Franzke, C.: Twentieth Century North Atlantic Jet Variability, Quarterly Journal of the Royal Meteorological Society, 140, 783–791, https://doi.org/10.1002/qj.2197, 2014.

Woollings, T., Barnes, E., Hoskins, B., Kwon, Y.-O., Lee, R. W., Li, C., Madonna, E., McGraw, M., Parker, T., Rodrigues, R., Spensberger, C., and Williams, K.: Daily to Decadal Modulation of Jet Variability, Journal of Climate, 31, 1297–1314, https://doi.org/10.1175/JCLI-D-17-0286.1, 2018a.

Woollings, T., Barriopedro, D., Methven, J., Son, S.-W., Martius, O., Harvey, B., Sillmann, J., Lupo, A. R., and Seneviratne, S.: Blocking and Its Response to Climate Change, Current Climate Change Reports, 4, 287–300, https://doi.org/10.1007/s40641-018-0108-z, 2018b.

Woollings, T., Drouard, M., O'Reilly, C. H., Sexton, D. M. H., and McSweeney, C.: Trends in the Atmospheric Jet Streams Are Emerging in Observations and Could Be Linked to Tropical Warming, Communications Earth & Environment, 4, 1–8, https://doi.org/10.1038/s43247-023-00792-8, 2023.

https://doi.org/10.5194/egusphere-2024-3029
Preprint. Discussion started: 8 October 2024

		DJF		MAM		JJA		SON		Year	
		1959-	1979-	1959-	1979-	1959-	1979-	1959-	1979-	1959-	1979-
Avg. longitude	STJ	−24	−50	**−44**	−25	14	−20	−6.9	−8.9	−22	−28
$[10^{-3}$ °E/year]	EDJ	**16**	20	**28**	**39**	0.22	−12	−8.2	−23	**8.9**	6.1
Avg. latitude	STJ	−1.5	1.5	−7.8	−12	−14	−8.2	7.1	**25**	**−6.7**	0.32
$[10^{-3}$ °N/year]	EDJ	8.8	5.9	11	11	−2.6	6.5	0.8	6.4	4.6	7.4
Avg. p. level	STJ	−1.8	−3	**−6.8**	2.4	**−7.5**	**−8.5**	**−5.9**	−3.2	**−5.3**	−2.5
$[10^{-2}$hPa/year]	EDJ	**−7.7**	**−9.4**	**−9.6**	−8.3	**−16**	**−20**	**−12**	**−16**	**−11**	**−13**
Max. speed	STJ	**3.5**	2.4	1.9	−2.9	**−3.3**	−3.2	**3.4**	**5.6**	**2.4**	0.98
$[10^{-2}$m · s^{-1}/year]	EDJ	**2.9**	3.8	**2.3**	**6.6**	1.2	−0.12	**2.8**	1.4	**2.3**	**2.9**
Avg. speed	STJ	1.4	0.75	1.2	−2.4	**−2.2**	−2	**2.4**	**4.1**	**1.4**	0.46
$[10^{-2}$m · s^{-1}/year]	EDJ	1.3	1.2	0.7	**3**	0.63	0.34	0.97	0.12	**0.9**	1.2
Tilt	STJ	−1.8	−2.4	**−5.2**	−0.19	1.8	−1.2	1.6	−4.6	−1.6	−2.3
$[10^{-4}$ °N/ °E/year]	EDJ	1.3	−5.2	1.8	−1.9	−2.6	−0.32	−3.3	−5.8	−0.71	−3.3
Linear waviness	STJ	5.3	7.1	**10**	3.3	3.9	6.9	−0.82	6.9	**5.3**	**5.8**
$[10^{-4}$ °N/ °E/year]	EDJ	−0.85	1.9	0.26	1.4	1.1	−3.4	1.9	3.4	0.59	0.84
R16 waviness	STJ	2.5	1.5	−3.4	**−14**	9.8	−0.42	12	15	4.2	−0.33
$[10^{-4}$ °N/ °E/year]	EDJ	59	85	23	−95	7.3	−79	**78**	36	**42**	−14
DC16 waviness	STJ	6.5	12	8	14	2.9	14	−3.4	4.6	4.8	11
$[10^{-4}$ /year]	EDJ	−1.7	2.5	−1.4	3.7	1.6	−3.2	0.18	−2.8	−0.33	0.071
FV15 waviness	STJ	**4.6**	0.02	−0.1	2.2	6.9	7.5	2.5	3	**2.8**	2.7
$[10^{-5}$ /year]	EDJ	−2.4	−7.4	1.3	−1.4	0.29	2.8	**−7.2**	**−14**	−2	−5
Width	STJ	**−1.8**	−1.6	−0.46	**−2.1**	**−1.1**	−1	**−0.9**	−0.33	**−0.84**	**−1.2**
$[10^{3}$m/year]	EDJ	**−0.62**	**−1.5**	−0.26	−0.43	−0.25	−0.11	−0.36	−0.52	**−0.37**	**−0.63**
Integrated speed	STJ	3.3	5.4	3.7	2.8	−0.63	2.5	0.95	**5**	2.7	4.3
$[10^{5}$m^2 · s^{-1}/year]	EDJ	1	2.5	0.83	3.6	0.89	−0.87	0.77	−0.88	0.87	1.1
Intd. speed over Eur.	STJ	1.1	0.62	−0.01	0.44	0.33	1.1	0.53	**3.1**	0.76	1.4
$[10^{5}$m^2 · s^{-1}/year]	EDJ	**1.1**	1.5	**1.2**	**2**	0.055	−1	−0.019	−1.1	**0.57**	0.34
Jet lifetime	STJ	2.3	−8.9	−5.5	12	−23	15	−7	−4.5	−7.9	2
$[10^{-3}$day/year]	EDJ	−0.23	−5.8	1	11	11	13	−1.6	−1.2	2.5	4.3
Speed of COM	STJ	−14	7.8	20	−4.9	−24	−17	−14	32	−4.3	6.9
$[10^{-3}$m · s^{-1}/year]	EDJ	−3.5	7.1	5.9	**23**	−11	2.1	**−14**	−18	−5.7	4
Double jet index $[10^{-4}$ /year]		**5.4**	8.2	**13**	**21**	−3.1	−1.2	−0.74	3.6	**3.6**	**7.9**

Table B1. Extended version of table 1.